

國立臺灣大學牙醫專業學院臨床牙醫學研究所

碩士論文

Graduate Institute of Clinical Dentistry

School of Dentistry

National Taiwan University

Master Thesis



人工植體頸部型態的差異對周圍骨質應變之影響

The Effect of Different Implant Neck Designs

upon Strain at Surrounding Bone

曾莉婷

Li-Ting Tseng

指導教授：林立德 副教授

Advisor: Li-Deh Lin, Associate Professor

中華民國102年7月

July 2013

國立臺灣大學碩士學位論文  
口試委員會審定書

人工植體頸部型態的差異對周圍骨質應變之影響

The Effect of Different Implant Neck Designs  
upon Strain at Surrounding Bone

本論文係 曾莉婷 (R99422007) 在國立臺灣大學牙醫專業學院臨床牙醫學研究所，補綴學組完成之碩士學位論文，於民國一百零二年七月十一日承下列考試委員審查通過及口試及格，特此證明

口試委員：

\_\_\_\_\_ (簽名)

(指導教授)

林弘光

張松

許明倫

系主任、所長

郭喜村

\_\_\_\_\_ (簽名)

## Acknowledgements



Three years as a graduate student in National Taiwan University Hospital eventually ends at this moment. I have been incredibly lucky to have two of the best supervisors one could hope for – Dr. Li-Deh Lin and Dr. Tsung-Chieh Yang. I am extremely grateful to Dr. Lin's endless support and invaluable guidance in both clinical experience and academic research. With your tutorial and encouragement, I have learned and grown a lot in the past three years. Dr. Yang has given me many instructions and discussed the details of the experiment with me patiently. I have been given so much freedom on this amazing and unforgettable journey.

I would like to give my sincere gratitude to all other instructors in Prosthetic department, Dr. Fen-Hui Lin, Dr. Juo-Song Wang, Dr. You-Chyun Hsu, Dr. Tong-Mei Wang, Dr. Ming-Shu Lee, Dr. Alex Yunn-Jy Chen, Dr. Yuh-Yuan Shiau and Dr. Chia-Yuan Hu. With your generous support, I have not only gained abundant precious knowledge and experience but also improved my thinking process and comprehensive view in prosthetic dental treatment. I also want to thank Dr. Sang-Heng Kok and Dr. Hao-Hueng Chang in Oral and Maxillofacial department. Without your direction and guidance, I will not have such a deep understanding of dental implant surgery. With all the help and care in this big family, I have enjoyed every moment of my training.

Last but not least, I owe my heartfelt appreciation to my parents, my sister, the whole family and my lovely friends. Your warm and firm support is my strongest backing to chase my goal and dream. Thank you for your selfless tolerance; this is my power to face every difficulty. This article is dedicated to my dearest mother, who is not able to see my graduation personally. I love you, mom.

# 人工植體頸部型態的差異

## 對周圍骨質應變之影響



**實驗目的：**在人工植牙的臨床應用上，牙醫師經常會面對不理想的骨質和骨量，造成治療上的困難，而植體的生物機械特性，就成為改善人工植牙預後的重要因素。學者進一步提出“功能性表面積”的想法來解釋在骨頭－植體交界面的應力傳導，然而，目前的研究對這個區域的細節還沒有全盤了解。本實驗的研究目的即希望能進一步釐清這個區域的範圍，並了解它是如何對應力分散造成影響。

**材料與方法：**本實驗中採用兩種不同設計的植體：Brånemark (Mk III, 瑞典) 植體的尺寸分別為直徑3.75或5.0 mm，長度8.5或10.0 mm。Astra Tech (OsseoSpeed, 瑞典) 植體的尺寸分別為直徑4.0S、5.0S或5.0 mm，長度9.0或11.0 mm。每種尺寸的植體有兩個樣本，每支植體被包埋在聚甲基丙烯酸甲酯樹脂塊 (85×20×30 mm) 中，藉以模擬上顎無牙區的低密度骨質。每支植體表面上黏有四個微型應變計 (KFG-02-120-C1, Kyowa, 日本)，測量點分別在植體平台以下1.0、2.0、4.0及5.0 mm的位置。在模擬支台齒的鈦金屬塊 (8×8×8 mm) 上施以30度，50牛頓的定力，每個模型6次，並記錄四個測量點的應變值。

**實驗結果：**所有植體平均應變值 (MSV) 的最大值皆出現在植體平台以下1.0 mm處，且較其他3個測量點達到顯著差異 ( $P < 0.05$ )。Brånemark組的MSV最大值出現在3.75\*8.5 mm的植體上，Astra Tech組的MSV最大值則出現在4.0S\*9.0 mm的植體上。當植體的直徑增加，或長度增加時，MSV有減少的現象，在兩組不同設計的植體上，直徑和長度的影響力並不相同。此外，植體的設計，包括微螺紋或外展等，都會對測量到的MSV造成影響。



**結論：** 在本實驗的條件限制下，無論植體的直徑、長度或設計，最大的應力集中都發生在植體平台以下2.0 mm的範圍。因此可以推論，有一個主要支持區在這個範圍，並且承擔了大部分植體受力時傳導下來的應變。而植體在這個區域內若有良好的設計，將會對應力分散給予更多的好處。

**關鍵詞：** 植體，電阻應變計，應變，植體頸部設計

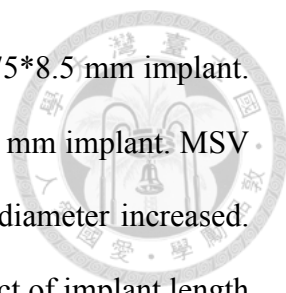
# The Effect of Different Implant Neck Designs upon Strain at Surrounding Bone



**Objectives:** During the clinical practice of implant treatment, dentists are usually bothered by facing unfavorable bone quantity and quality. The implant biomechanic characteristics become important to improve the prognosis of implant placement. Therefore, the idea of “functional surface area” was brought up to explain more about stress transferring at bone-implant interface. Unfortunately, we did not really understand the details of this area. The aim of the present study was to identify this area and how it influences the stress distribution.

**Methods:** Two different designs of dental implants were included in this study. The sizes of Brånemark (Mk III, Sweden) implants were 3.75 or 5.0 mm in diameter and 8.5 or 10.0 mm in length. The sizes of Astra Tech (OsseoSpeed, Sweden) implants were 4.0S, 5.0S or 5.0 mm in diameter and 9.0 or 11.0 mm in length. There were two implants of each size. Each implant was embedded in a polymethyl methacrylate resin block (85 X 20 X 30 mm), simulating a maxillary edentulous region with low-density bone. Four miniature strain gauges (KFG-02-120-C1, Kyowa, Japan) was attached to each implant where the measuring points were at 1.0, 2.0, 4.0 and 5.0 mm below the platform on the external surface of the implant. A 30-degree oblique static load of 50N was applied 6 times on a Ti block (8 X 8 X 8 mm) screwed on the implant of each model and bone strains at the four measuring points were recorded.

**Results:** All implants showed the largest mean strain value (MSV) at 1.0-mm site below the platform which was statistically higher ( $P < 0.05$ ) than the other 3 measuring



sites. For Brånemark implants, the largest MSV was observed in 3.75\*8.5 mm implant. For Astra Tech implants, the largest MSV was observed in 4.0S\*9.0 mm implant. MSV decreased when the implant length increased and when the implant diameter increased. However, difference existed between two implant designs in the effect of implant length and implant diameter on MSV. The outspreaded or microthreaded design also affected the MSV.

**Conclusion:** Within the limitation of this in-vitro study, we concluded that MSV concentrated mostly at 2.0 mm below platform of implants in different diameters, lengths or designs. Therefore, there was a primary supporting area in peri-implant bone where received most strain from implants during loading. Well design in this area would give more benefits in stress distribution.

**Key words:** implant, strain gauge, strain, implant neck design

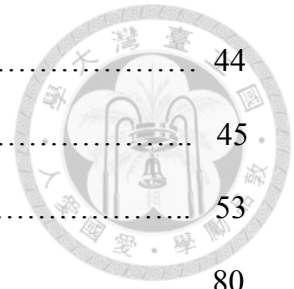
# Table of Contents



Verification letter from the Oral Examination Committee.....	I
Acknowledgement.....	II
摘要.....	III
Abstract.....	V
Table of Contents.....	VII
List of Figures.....	IX
List of Tables.....	XI
Chapter 1 Introduction.....	1
Chapter 2 Literature Review.....	2
2.1 Success Rate.....	2
2.2 Mechanostat Theory.....	4
2.3 Relationship Between Nature of Force and Bone Cell.....	5
2.4 Stress Dispersion of Implant Under Force.....	5
2.5 Functional Surface Area.....	7
2.6 Primary Support Area.....	8
2.7 Implant Type and Design.....	9
2.8 Methods to Measure Stress Variation Around Dental Implant.....	15
Chapter 3 Motivation and Purpose.....	19
Chapter 4 Materials and Methods.....	20
Experiment 1: Different positions of the same implant.....	20
Experiment 2: The effect of implant diameters and lengths.....	26
Experiment 3: The effect of implant designs.....	27
Chapter 5 Results.....	29
Chapter 6 Discussion.....	34



Chapter 7 Conclusion.....	44
Reference.....	45
Figures.....	53
Tables.....	80

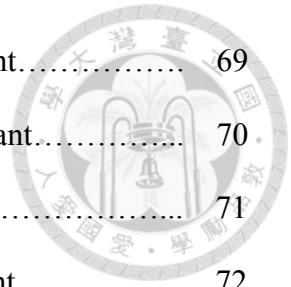


# List of Figures



Fig. 1: Diagram of Mechanostat Theory.....	53
Fig. 2: Different intensity of cortical bone response.....	53
Fig. 3: Primary supporting area by Yang et al. (2001).....	54
Fig. 4: The basic macrothread structures of dental implants.....	54
Fig. 5: The structural diagrams of implants in this experiment.....	55
Fig. 6: Remove excess PMMA resin on the implant surface.....	55
Fig. 7: Brånemark implant covered with resin after polishing.....	56
Fig. 8: Astra Tech implant covered with resin after polishing.....	56
Fig. 9: Diagram of micro-strain gauge.....	57
Fig. 10: Paste the strain gauge on the scaled table.....	57
Fig. 11: Brånemark implant with strain gauges pasted.....	58
Fig. 12: Astra Tech implant with strain gauges pasted.....	59
Fig. 13: Strain gauge coated with the thermal insulation.....	60
Fig. 14: 85*20*30 mm <sup>3</sup> rectangular block of die stone.....	60
Fig. 15: The model mode made of additional silicone.....	61
Fig. 16: The main body of PMMA resin model.....	61
Fig. 17: Device of model fabrication.....	62
Fig. 18: Brånemark model with 8*8*8 mm <sup>3</sup> titanium abutment.....	62
Fig. 19: Metal stage design.....	63
Fig. 20: Loading machine.....	64
Fig. 21: Signal convertor.....	65
Fig. 22: Cartoon diagram of the model and force.....	66
Fig. 23: MSV and decreasing rate of 5.0*8.5 mm Brånemark implant.....	67
Fig. 24: MSV and decreasing rate of 5.0*10.0 mm Brånemark implant.....	68

Fig. 25: MSV and decreasing rate of 3.75*8.5 mm Brånemark implant.....	69
Fig. 26: MSV and decreasing rate of 3.75*10.0 mm Brånemark implant.....	70
Fig. 27: MSV and decreasing rate of 5.0*9.0 mm Astra Tech implant.....	71
Fig. 28: MSV and decreasing rate of 5.0*11.0 mm Astra Tech implant.....	72
Fig. 29: MSV and decreasing rate of 5.0S*9.0 mm Astra Tech implant.....	73
Fig. 30: MSV and decreasing rate of 5.0S*11.0 mm Astra Tech implant.....	74
Fig. 31: MSV and decreasing rate of 4.0S*9.0 mm Astra Tech implant.....	75
Fig. 32: MSV and decreasing rate of 4.0S*11.0 mm Astra Tech implant.....	76
Fig. 33: The effect of diameter and length in Brånemark group.....	77
Fig. 34: The effect of diameter and length in Astra Tech group.....	77
Fig. 35: Comparison of Brånemark and Astra Tech groups.....	78
Fig. 36: The effect of outspreaded design.....	78
Fig. 37: The test set-up suggested by ISO.....	79
Fig. 38: Dynamic bite force by Shimada et al.....	79



## List of Tables

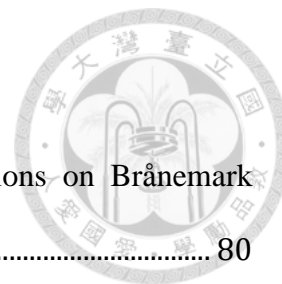


Table 1 : MSV and standard deviation of 4 different grid positions on Brånemark 5.0*8.5 implant.....	80
Table 2: MSV and standard deviation of 4 different grid positions on Brånemark 5.0*10.0 implant.....	80
Table 3: MSV and standard deviation of 4 different grid positions on Brånemark 3.75*8.5 implant.....	81
Table 4: MSV and standard deviation of 4 different grid positions on Brånemark 3.75*10.0 implant.....	81
Table 5: MSV decreasing rate in Brånemark group.....	82
Table 6: MSV and standard deviation of 4 different grid positions on Astra Tech 5.0*9.0 implant.....	82
Table 7: MSV and standard deviation of 4 different grid positions on Astra Tech 5.0*11.0 implant.....	83
Table 8: MSV and standard deviation of 4 different grid positions on Astra Tech 5.0S*9.0 implant.....	83
Table 9: MSV and standard deviation of 4 different grid positions on Astra Tech 5.0S*11.0 implant.....	84
Table 10: MSV and standard deviation of 4 different grid positions on Astra Tech 4.0S*9.0 implant.....	84
Table 11: MSV and standard deviation of 4 different grid positions on Astra Tech 4.0S*11.0 implant.....	85
Table 12: MSV decreasing rate in Astra Tech group.....	85
Table 13: Collinearity diagnosis of diameter and length in Brånemark group: by (a) correlation coefficient and (b) Condition Index.....	86

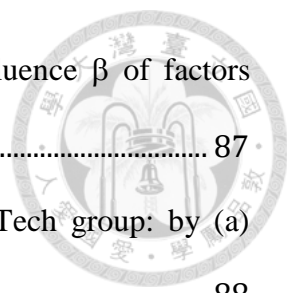
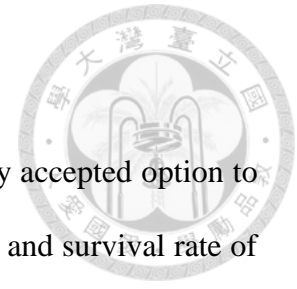


Table 14: (a) coefficient of determination  $R^2$  and (b) variable influence  $\beta$  of factors  
diameter and length in Brånemark group..... 87

Table 15: Collinearity diagnosis of diameter and length in Astra Tech group: by (a)  
correlation coefficient and (b) Condition Index..... 88

Table 16: (a) coefficient of determination  $R^2$  and (b) variable influence  $\beta$  of factors  
diameter and length in Astra Tech group..... 89

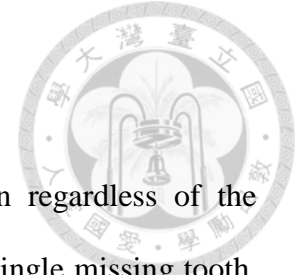
# Chapter 1 Introduction



During the past fifty years, dental implantation has become a widely accepted option to restore missing teeth for both dentists and patients. The success rate and survival rate of this treatment are above ninety percent regardless of its application on single missing tooth, partially edentulous area or fully edentulous area. The factors contributing to the implant success rate can be generalised into five classifications: host, biological factors, surgical factors, implant design and biomechanical factors. Among these factors, implant design and biomechanical factors are the two main factors related to mechanics. When an occlusal loading force is applied on a dental implant, in addition to the implant itself, this force is expected to be transferred, through a proper implant design, toward the surrounding bone. In consequence, both implant and bone have to share and withstand the stress loaded and avoid mechanical failure due to stress concentration on either the bone or implant.

Furthermore, bone quality at the patient's implant placement sites is important for biomechanical properties of implant-bone interface. Ideally, dentists should place implants at the surgical area where the bone quality and quantity are well and sufficient. However, not all patients have such proper conditions at implant sites. For example, chronic periodontitis and/or missing teeth for a long time would cause a large amount of alveolar bone resorption at implant sites. Whether we can reduce the amount of stress concentration at implant-bone interface and decrease biomechanical risks by changing the length, width or design of the implant has become a topic of concern. Therefore, in this study, strain gauges were used to measure and analyze stress changes around the implant under different factors.

## Chapter 2 Literature Review




Currently, dental implantation is a widely used treatment option regardless of the application to a fully edentulous area, partially edentulous area or single missing tooth. It is a predictable dental treatment with good prognosis and widely accepted by both dentists and patients.

### 2.1 Success Rate

Success criteria for dental implants, which is highly accepted and used today, were proposed by Albrektsson et al. (1981) as follows: no mobility under clinical examination, no radiolucency of image around the implant, amount of annual bone loss should be less than 0.2 mm after one year of implant placement and no continuous or irreversible symptoms and signs such as pain and infection.

According to a literature review in 1997 (Buser et al., 1997), the earliest long-term clinical follow-up report of osseointegrated implants was a retrospective study on Brånemark implants, applied to fully edentulous patients (Adell et al., 1981, 1990). The 15-year implant survival rates were 86% at mandible and 78% at maxilla. Several prospective clinical studies were reported thereafter. In the study of Zarb and Schmitt (1990a, b, c), 274 implants were applied to fully edentulous patients to support 49 sets of overdentures. The success rate of implant osseointegration was 89.05%, and the success rate of functional use of dentures was 100%. Buser et al. (1997) reported 2359 ITI implants, from several medical centres, in 1003 patients with single missing tooth, partially edentulous area or fully edentulous area. The 5-year implant survival and

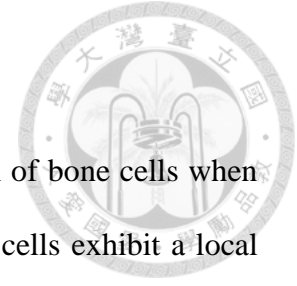


success rates were 98.2% and 97.3%, respectively. The 8-year implant survival and success rates were 96.7% and 93.3%, respectively. Weibrich et al. (2001) followed 515 Astra Tech implants in either partially or fully edentulous patients. The 5-year implant survival rate was 95.9% and the success rate was of 85%. Artzi et al. (2006) studied 248 hydroxyapatite-coated implants in 62 patients; they reported a 5-year survival rate of 94.4% and a success rate of 89.9%. The 10-year survival and success rates were 92.8% and 54%, respectively. Gotfredsen (2012) conducted a long-term trial for maxillary anterior single implant (Astra Tech). The 10-year survival rate of the implant was 100%, whereas the survival rate of crown was 90%.

Host, biological factors, surgical factors, implant design and biomechanical factors are the five major elements affecting the survival and success rate of dental implants (Karoussis et al., 2004). Host factors include systemic diseases of patients, such as osteoporosis, radiation therapy, diabetes mellitus or bad habits of patients (e.g. smoking) (Genco et al., 2001). Biological factors are mostly related to microbiota, such as peri-implantitis. Surgical factors may be overheating during surgery, which can cause bone necrosis or incorrect diagnosis by surgeons. Implant design was emphasised by Rieger et al. (1989), who reported that high stress concentration must be avoided at the implant neck to minimize the crestal bone resorption. Biomechanical factors are related to how the loading force spreads (Tonetti and Schmid, 1994; Tonetti, 1998). Among these five factors, implant design and biomechanical factors are highly related to the intersurface between the implant and bone. Therefore, the reaction of bone cells under stress must be understood.



## 2.2 Mechanostat Theory



A threshold-based mechanism was proposed to explain the reaction of bone cells when bone tissue is under stress. Mechanostat theory suggests that bone cells exhibit a local reaction toward mechanical stress (Frost, 1987).

Four-staged reactions occur toward the micro-stress of the interface between a dental implant and surrounding bone (Fig. 1). Acute disuse window leads to bone resorption. Adapted window is a balanced condition of bone resorption and regeneration. The outlined form of bone tissue is maintained at this phase in comparison with increased bone density. Mild overload window compensates for fatigue fractures by repairing woven bone. Pathologic overload window causes fatigue fractures and bone resorption. In addition, the reaction between stress and reaction of bone tissue is not a linear relationship.

According to Nicoletta et al. (1997), the amount of strain, which caused 0.15% of deformation detected by the strain gauge on the bone sample, can actually cause 3.5% of deformation on other microstructures. The speed of bone remodelling may be the explanation because bone cell membrane can react as a mechanosensory system in bone (Cowin et al., 1991). Thus, the behaviour of bone cells is mainly affected by the mechanical environment or deformation of bone cells (Rubin et al., 1988; Brighton et al., 1991). Sachs (1988, 1991) further speculated that the energy source to open ion membrane channels on the bone cell membrane is gained from the micro strain produced by the loaded bone.



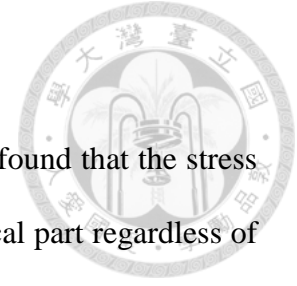
### **2.3 Relationship between Nature of Force and Bone Cell**

Nature of force is an important factor that must be considered when discussing about the impact of biomechanical factors upon the implant success rate (Misch, 2004). The directions of force applied on teeth can be characterised into vertical positive force and horizontal shear force. Three major kinds of force should be discussed: compressive force, tensile force and shear force.

Cortical bone reacts differently against these three kinds of forces. It has the strongest resistance to compressive force with 30% decrease to tensile force and 65% decrease to shear stress (Cowin and Mehrabadi, 1989) (Fig. 2). Moreover, bone tissue shows different resistances to varied angles of force. The strongest resistance appears when compressive force or tensile force passes the long axis of bone tissue; bone resistance decreases by 11% to compressive force and 25% to tensile force with 30-degree force (Misch and Bidez, 1994).

### **2.4 Stress Dispersion of Implant under Force**

The result 'dispersion of stress is not even at different sites of implant' has been proven by many scholars. Rieger et al. (1990) and Bidez and Misch (1992) examined stress dispersion using finite element method (FEM) and photoelastic analysis. The crestal zone has the most important impact upon stress dispersion, and the implant cervical area has the highest stress concentration when an implant is under force.



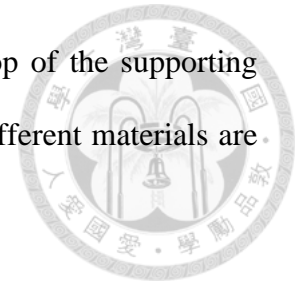
Pierrisnard et al (2003) analysed implants (6-12 mm) via FEM and found that the stress gradually decreases along the implant from the neck area to the apical part regardless of the implant length. Moreover, the stress around the implant gradually decreased as the length increased on the 6-8 mm unicortical anchorage implant. However, when the implant length exceeded 8 mm, increased implant length caused 16.8% higher stress on the 8-12 mm implant. A 29% increase in stress was noted on the 12 mm bicortical anchorage implant.

Bozkaya et al. (2004) analysed five different thread types of implants by FEM and found overloading on the top of the bone under extremely huge biting force (more than 1000N). The geometric pattern of the implant crestal module was suggested to be highly important to reduce stress conducting to bone tissue. Schrotenboer et al. (2008) analysed different types of implant crestal module, including microthreads and smooth neck, by 2D FEM. Their results showed that the stress concentration is mainly at the top of the crestal bone, regardless of implant design.

Hoshaw et al. (1994) and Duyck et al. (2001) placed dental implants in jawbones of dogs. Both teams found the most obvious bone loss occurred at the implant neck when screw-type implant was under vertical tensile force.

Isidor (2006) placed implants in jawbones of monkeys and analysed histomorphometrically. Their results showed that pressure conducts to bone when the

implant is under biting force, and the highest pressure is at the top of the supporting bone. The highest stress occurs at the first contact site when two different materials are in contact with each other when one of them is under force.



Thus, when an implant is under force, instead of even dispersion to the whole implant, pressure will concentrate at the top of the supporting bone while the implant neck will be the location of stress concentration.

## **2.5 Functional Surface Area**

In terms of the biomechanics of implants, instead of focusing on the total surface area, dentists focus on the main area that can bear and disperse force, that is, functional surface area. Dr. Misch officially introduced this concept in 2004. When an implant is under loading, functional surface area is the area that can actively disperse non-shear force, such as compressive force and tensile force, by the implant-to-bone interface. Functional surface area also provides initial stability during surgical implant placement. Specifically, it is the part of the thread that participates in stress dispersion, namely, functional thread surface area.

At implant site with different bone qualities, functional surface area may cause variations in the implant-bone contact area. Threaded, root form titanium implant in the hardest D1 bone has about 80% bone tissue at the implant interface at the initial healing stage. The percentage of bone tissue gradually decreases in softer bone such as D2 and D3 and is merely 25% in D4 bone (Misch, 1990). Therefore, functional surface area per

unit of implant length must be increased to decrease mechanical stress in poor quality bone areas (Misch, 2004).



In the experiment of Tada et al. (2003), the apical part of long implants may have less stress conduction because the highest stress concentration is located at the crestal bone area where enhanced bone resorption occurs. The need for functional surface area increases gradually when the bone quality becomes worse from D1 bone to D4 bone.

Although the importance of functional surface area to dental implant is confirmed, the details of this area remain unclear. Extensive research has been conducted to understand this area ever since Misch proposed this concept. The concept of primary supporting area was also produced under the same premise.

## **2.6 Primary Support Area**

Yang et al. (2011) proposed this concept according to their experiments: on single implant, the decrease in mean strain value (MSV) at 1 mm under the implant platform is statistically significant when the implant diameter increases; the same condition becomes evident when two implants are connected. Therefore, the diameter of the implant influences stress dispersion. However, the difference in MSV between two connected 7 mm short implants and one 12 mm long implant connected to one short implant is less than  $4 \mu\epsilon$  and can be ignored (Fig. 3).

Therefore, Yang et al. (2012) suggested that an area under the platform needs to be redefined. It is the main site of stress concentration when an implant is loaded, and it functions as primary supporting area of an implant with important impact upon stress dispersion. Variations in implant condition within this area, such as larger diameter, affect stress dispersion more than increasing length beyond this area. Meanwhile, Yang et al. reported the limitation of using only one micro-resistance strain gauge to record the strain value in their experiments and suggested that more information about the range and usage of primary supporting area would be obtained if the numbers and locations of the strain gauge increase in further experiments.

## **2.7 Implant Type and Design**

The earliest osseointegrated implant design was traced to 1965, when Brånemark used pure titanium to create a V-shaped threaded screw type. Self-tapping implants were designed to put into softer bone since 1983. The ideal implant design offers satisfactory initial stability and sufficient strength to conduct biting force (Cooper, 2000). Various strain characteristics of supporting bone surrounding different implant designs were also determined by *in vivo* experiments (Pilliar et al., 1991). Therefore, to gain better biomechanical characteristics, the present research focuses on the tolerance of biting force and adaptation of different bone densities (Binon et al., 2000).

Implant design can be generally classified into two types: macrodesign and microdesign. Macrodesign (Fig. 4) includes screw, implant form and thread design (Geng et al., 2004), whereas microdesign includes implant material, surface morphology and surface

coating. This experiment discusses mainly about the biomechanics of dental implants, which is related to macrodesign.

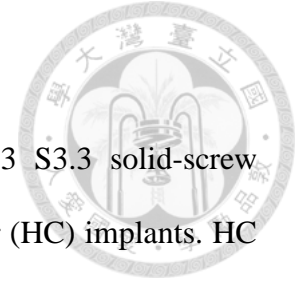


According to the literature review of Abuhussein et al. (2010), the geometric pattern of implant thread is related to stress dispersion around an implant. Decreasing thread pitch positively affects the stability of an implant. A large thread helix angle fastens the insertion of an implant but may endanger the ability of the implant to support axial force. Thread depth may have an important impact upon implant stability in poor bone quality area. Increasing threads or microthreads to the top of the implant neck may provide a potentially positive effect on the contact between bone and implant and maintain marginal bone simultaneously. However, all these results need further experiments and evidence.

#### **A. Implant Form:**

Although many different shapes of root form endosteal implants have been developed during the past forty years, cone shape is still the mainstream. Nevertheless, it can be subdivided into three types, namely, threaded screw, coated cylinder and hollow-basket cylinder. Furthermore, most currently commercialized implants are threaded screw ones.

Siegele and Soltesz (1989) found that screw-shaped and full-body cylindrical implants produce less strain in comparison with implants with a small radius of curvature, such as conical, geometric discontinuity (stepped) or hollow-cylinder shape.



Buser et al (1997) studied 1141 S4.1 solid-screw implants, 213 S3.3 solid-screw implants, 639 hollow-screw (HS) implants and 366 hollow-cylinder (HC) implants. HC had the highest 7-year implant failure rate (8.7%), followed by HS (4.2%); solid-screw implants had the lowest failure rate at 3.2%.

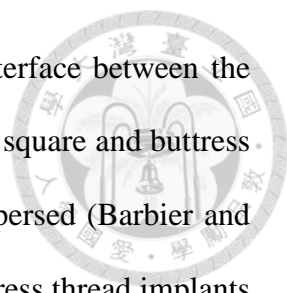
Karoussis et al. (2004) reported a 10-year follow up of ITI system in 89 patients with 112 HS implants, 49 HC implants and 18 angulated hollow-cylinder (AHC) implants. The 10-year implant survival rates were 95.4%, 85.7% and 91.7% in HS, HC and AHC groups, respectively. The success rate varied considerably due to different conditions. However, HS design exhibited a statistically higher 10-year survival rate and lower incidence rate of peri-implantitis compared with other designs.

In conclusion, implant form with screw type, which is currently the most popular implant design, leads to smaller strain and higher implant survival rate than cylinder type.

## **B. Thread Shape:**

Thread shape can be divided into V-thread, square thread, buttress thread, reverse buttress thread and spiral thread.





The angle of the thread can change the direction of force at the interface between the bone and implant (Bumgardener et al., 2000). Axial force loaded on square and buttress thread implants is transformed into compressive force and then dispersed (Barbier and Schepers, 1997; Bumgardner et al., 2000); V-thread and reverse buttress thread implants disperse axial force via compressive, tensile and shear forces (Misch, 2008). Square thread implants exhibit better bone-to-implant contact and higher reverse torque than V-thread and reverse buttress thread implants (Steigenga et al., 2004).

### **C. Thread Pitch:**

Implants with more threads, which mean smaller thread pitch, have higher percentages of bone-implant contact (Roberts et al., 1984). According to results from 3D FEM, implants with 0.8 mm thread pitch displayed stronger resistance to vertical force than 1.6 mm and 2.4 mm thread pitch (Ma et al., 2007). The maximum value of effective stress decreases when thread pitch decreases or implant length increases (Chun et al., 2002; Motoyoshi et al., 2005). Chung et al. (2008) found that implants with 0.6 mm thread pitch have more crestal bone loss than implants with 0.5 mm thread pitch; stress dispersion is enhanced on the implant surface when thread pitch decreases. However, not all experiments support this result. Kong et al. (2006) showed that cylinder implants with 0.8 mm thread pitch and V-thread shape can achieve the best initial stability and stress distribution; either a smaller or larger thread pitch than 0.8 mm would produce more stress. They also found that stress is more sensitive to thread pitch in sponge bone than in cortical bone. Thread pitch protects the implant better under axial force than under non-axial force, such as force from the buccal or lingual side.



#### **D. Thread Helix Angle:**

Thread helix angle may change according to the number of thread helix, from single to double- or triple-helix thread (Abuhussein et al., 2010).

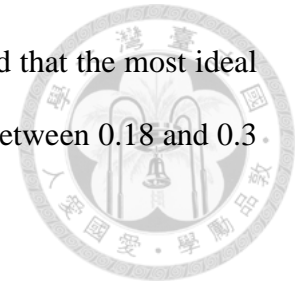
Ma et al. (2007) analysed 0.8 mm thread pitch implants with single, double- and triple-helix thread by FEM. Their results showed that single thread exhibits the best implant stability, followed by double-helix thread. Triple-helix thread implant displays the worst implant stability among the three types, although it demonstrates rapid insertion. Therefore, emphasis on ease of implant insertion may sacrifice initial stability of the implant simultaneously.

#### **E. Thread Depth and Width:**

Thread depth refers to the distance between the major diameter and minor diameter of the screw (Misch, 2008), and it is also called thread height. Thread width refers to the distance between the top and bottom edges of the tip of a single thread at the same axial plane (Abuhussein et al., 2010).

Implants with deep thread depth are suitable for low-density bone and high occlusal load due to the large functional surface area with bone. By contrast, implants with narrow thread width can be easily inserted into bone with high density and need less tapping before insertion (Misch, 2008).

Kong et al. (2006) analysed V-thread implant by 3D FEM and found that the most ideal thread depth is between 0.34 and 0.5 mm, whereas thread width is between 0.18 and 0.3 mm. Peak stress is more sensitive to thread depth than thread width.



#### **F. Microthreads:**

Microthreads are threads with minute, fine and shallow profiles. They have been developed for use at the crestal area to maintain marginal bone and soft tissue around an implant neck. Vaillancourt et al. (1995) mentioned that bone loss at the crestal area is caused by disuse atrophy. A smooth neck design causes minimal force conducted to the marginal bone and leads to bone resorption. Fixture MicroThread™, a microthread design developed by Astra Tech implant system, has a triple-threaded structure with 0.2 mm thread pitch compared to the general macrothread with 0.5-1.2 mm thread pitch.

Schrotenboer et al. (2008) found that a microthread design, compared with a smooth neck design, increases stress at the crestal area when an implant is under loading using 2D FEM. Palmer et al. (2000) also proved that retentive elements at the implant neck can maintain the height of the marginal bone. Abrahamsson and Berglundh (2006) observed implants inserted for 10 months in dog models and found that bone-implant contact at the microthread group is 81.8% compared with 72.8% in the non-microthread group.

According to Lee et al. (2007), when an implant is under loading, increasing retentive elements, such as microthread, at the crestal area may statistically significantly prevent

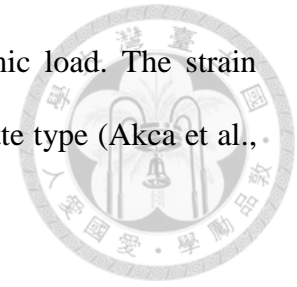
marginal bone loss. The controversial issue in this experiment was that implants with microthread design are tapered at the crestal area, which indicates a large diameter at the top. Despite this controversial issue, Lee et al. maintained that adding thread or microthread to the crestal module exerts potentially positive effects on bone-implant contact and marginal bone retaining.

## **2.8 Methods to Measure Stress Variation around Dental Implant**

Biomechanical analytic methods currently used in implant research include photoelastic analysis, 2D or 3D FEM, 2D or 3D mathematical/ geometric analysis and electrical resistance strain gauge (Akca et al., 2002). 3D FEM and strain gauge measurements have been more popular recently.

Finite element analysis establishes a mathematical model on computer, imports parameters to simulate real oral conditions (such as alveolar bone environment around an implant and amount and direction of force) and obtains a trend of stress variation shown by different colours. Given that the results obtained from FEM are from mathematical expressions, the accuracy of its prediction should be verified (Akca et al., 2002). Fabricating a model of the entity, which is deformed under loading, is required for strain gauge measurement. The strain gauge attached on the model detects deformation and produces a potential difference by a slight change in metal coil resistance. Wheatstone bridge circuit can measure resistance changes accurately. The potential difference can be converted into the strain and then the stress value according to the elasticity formula. This method can be used in either *in vivo* or *in vitro*

experiments; the stress source can be either static load or dynamic load. The strain gauge usually used is either uniaxial type or biaxial 60-degree rosette type (Akca et al., 2002).



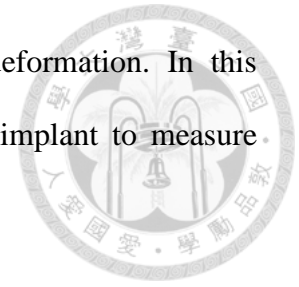
On one hand, the advantage of FEM is it can import multiple parameters to simulate clinical conditions; however, the disadvantage is that the result is a trend of change and a clear strain value cannot be obtained. Moreover, whether the parameter imported truly reflects the clinical situation remains unclear. On the other hand, exporting a strain value directly is the advantage of strain gauge, but the value only represents stress variation at the place the strain gauge is attached and not the entire sample. Considering the complication of model fabrication, real clinical situations are difficult to simulate. Given the absence of an ideal experimental method, some scholars have attempted to compare the accuracy of various techniques. Akca et al. (2002) compared strain gauge and two different settings of 3D FEM (strain gauge model and human alveolar bone model) and found that strain gauge has a higher strain value than the two different settings of FEM. However, the distribution and position of strain in the strain gauge group are similar to those in the FEM group. Akca et al. (2002) revealed that the FEM model assumes implant and abutment are single homogeneous objects and does not consider variables, such as thread, every interface between each component, torque of prosthesis and suitability. The use of a strain gauge requires highly technical skills, and positioning the strain gauge at exactly the same position on each model is almost impossible. Thus, the models of these two methods are not accurate enough to represent clinical conditions.

Cehreli et al. (2004) used photoelastic analysis and strain gauge to compare the differences in force conducting at the bone-implant interface with various implant designs. They found that photoelastic analysis cannot identify stress distribution at the microthread area; a three-leaf strain gauge can detect 2D deformation but can only be attached on the surface of the model close to the implant instead of the implant surface due to its large size. In addition, strain value would plummet if the strain gauge becomes loose during force loading.

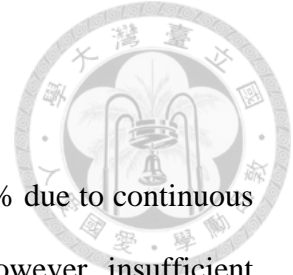
In general, the strain gauge can be placed in two positions for stress experiments with implants. One is on the surface of models (Akca et al., 2002, 2008; Abduo et al., 2012), which can be easily fabricated. However, the value measured cannot represent the actual change on the surface of measuring objects due to the embedded material in between. The other is on the surface of measuring objects (Cehreli et al., 2004; Nissan et al., 2010; Yang et al., 2011) and embedded in the model with objects together. The advantage of this method is it can accurately measure stress change at the desired position. The disadvantages of this method include increased difficulty of model fabrication, and heat released during model polymerisation may affect the accuracy of the strain gauge.

Kawara et al. (2008) aimed to confirm whether the measured value of the latter method is representative of the deformation of an object and is not affected by the exothermic reaction of embedded material. They found that the linear coefficient of thermal expansion of the sample calculated from the strain gauge in the resin is almost the same as the result calculated on the test piece. Therefore, the strain obtained by the strain

gauge embedded in the model is sufficient to reflect sample deformation. In this experiment, the strain gauge was attached on the surface of the implant to measure changes in stress at the interface between implant and bone.



## Chapter 3 Motivation and Purpose



The long-term success rate of dental implants has achieved over 90% due to continuous research and improvement in both implant types and materials. However, insufficient bone quality and quantity (e.g. large amount of alveolar bone resorption, insufficient distance to maxillary sinus or inferior alveolar nerve and concavity at maxillary anterior root tip area) are common in clinical conditions and lead to increased complexity and difficulty of surgery and the impact upon implant prognosis.

Therefore, for patients with unfavorable conditions, improving stress distribution via enhanced biomechanics of dental implants is important to increase the success rate. If more details of primary supporting area and the impact of implant designs at this area upon stress distribution are known, further prediction and analysis, such as the minimal bone height to achieve a good prognosis, can be obtained. Thus the purposes of this experiment were:

1. Defining a more specific range of primary supporting area, e.g. the primary area to support and distribute stress on an implant.
2. Advancing the use of primary supporting area by understanding the impact of implant designs and variations at this area upon stress distribution.



## Chapter 4 Materials and Methods



### **Experiment 1: Comparing the stress at different sites of the same implant.**

#### I. Dental implants: (Fig. 5)

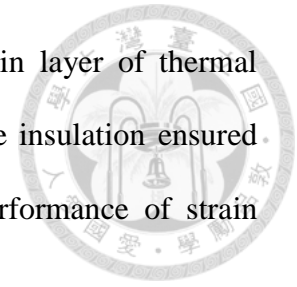
- A. Brånemark System (Mark III, TiUnite, Nobel Biocare, Gothenburg, Sweden): 3.75 mm (RP) and 5.0 mm (WP) in diameter; 8.5 and 10.0 mm in length. There were two implants with each size, eight implants in total.
- B. Astra Tech (OsseoSpeed, Mölndal, Sweden): 5.0, 5.0S and 4.0S mm in diameter; 9.0 and 11.0 mm in length. There were two implants with each size, twelve implants in total. Among these implants, the top of the 5.0 mm implant was a divergent design. Thus, the diameter of the implant platform was 5.0 mm, compared with the 4.0-mm implant body.
- C. The powder and liquid of polymethylmethacrylate (PMMA) (Ortho-Jet™, Lang, Wheeling, USA) were evenly mixed with a volume ratio of 20:1 (suggested by the manual). The mixture was poured into a container slightly larger than the implant, followed by putting the implant in. The container was left still in a pressure cooker for an hour to achieve complete polymerisation. Then took the implant, which was totally covered by PMMA, out.
- D. The implant was tightened with the metal axis of open tray impression coping (Brånemark open tray impression coping, Nobel Biocare, Gothenburg, Sweden; Astra Tech implant impressions pick-up, Mölndal,

Sweden) and the axis was put into a mechanical hand piece as a bur axis. Put a rasp beneath the implant (Fig. 6) and removed excess PMMA resin to a layer of 0.3 – 0.45 mm thick around the implant surface with the high-speed rotated technical hand piece. After that, polished its surface with sandpapers to gain a smooth cylinder (Fig. 7, 8).

## II. The choice and attachment of micro-strain gauges:

- A. The micro-strain gauge used in this experiment was KFG-02-120-C1-11L3M2R, Kyowa, Tokyo, Japan. Its base length was 3 mm, gauge length was 0.2 mm and resistance was 120  $\Omega$ . It could detect 1D plane deformation and connected with two 3-meter-long wires. It also had temperature compensation (Fig. 9).
- B. Adhesive: CC-33A cement (suggested by manufacturers of Kyowa).
- C. Attached positions: 0 and 3.0 mm beneath the implant platform on the same vertical line and 1.0 and 4.0 mm on the other vertical line which was at 180° opposite side. Therefore, each implant had four strain gauges attached, which were 0, 1.0, 3.0 and 4.0 mm beneath the implant platform; the positions of the grid (i.e. the actual measured position of strain) were at 1.0, 2.0, 4.0 and 5.0 mm beneath the platform. The implant was fixed on a double-sided hollow table (to let the wires through) to paste strain gauges. Both sides of the table were marked with a scale to ensure each paste position was on the same basis (Fig. 10).
- D. Strain gauges were set for 24 hours to ensure that the adhesive was completely hardened and fixed (Fig. 11, 12).

E. The surface of the strain gauge was coated with a thin layer of thermal insulation suggested by the manufacturer (Fig. 13). The insulation ensured that the exothermic temperature did not affect the performance of strain gauges when the PMMA resin polymerised.

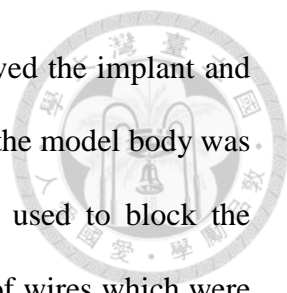


### III. Producing molds for experimental models:

First, a 85\*20\*30 mm<sup>3</sup> rectangular block was made with die stone and a 20\*20\*20 mm<sup>3</sup> cube was removed in the middle (Fig. 14). Then embedded this rectangular block with additional silicone. The model-making mold was obtained after removing the gypsum block (Fig. 15).

### IV. Fabrication of experimental models:

- A. The powder and liquid of PMMA were mixed evenly with a volume ratio of 20:1 and the mold (gained in step III) was put on a vibrator. Poured the mixture of PMMA into the mold and stood the mold still for an hour in a pressure cooker. This was the main body of the model after complete polymerisation (Fig. 16).
- B. Put the model body on a surveyor table and connected implants with their own metal axes of impression copings (Brånemark open tray impression coping, Nobel Biocare, Gothenburg, Sweden; Astra Tech implant impressions pick-up, Mölndal, Sweden). Ensured the axes were fixed to the horizontal arm of the surveyor so the implants were perpendicular to the model body.
- C. The prosthetic screwdriver was fixed with the metal crossbar. They were then set in the Inlay pattern resin (DuraLay<sup>TM</sup>, Reliance, Worth, USA) stands.

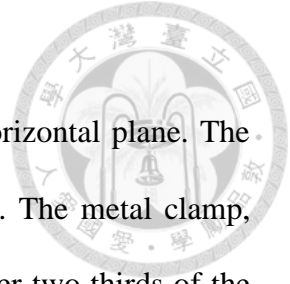


Unscrewed the horizontal arm of the surveyor and removed the implant and the model body. The relative position of the implant and the model body was fixed at this moment. Spatulas and paraffin wax were used to block the central hollow of the model body and fix the positions of wires which were connected to strain gauges (Fig. 17). Checked the perpendicularity of the implant and the model body again by putting them back to the surveyor.

- D. Tightened the abutment tooth to prevent excess resin flowing into the implant and lead to an inaccurate screw location.
- E. Mixed the powder and liquid of PMMA evenly with a volume ratio of 20:1 and layered the mixture into the central hollow of the model body. Separator (Ortho-Jet™, Lang, Wheeling, USA) of PMMA resin was applied at the part beyond the hollow to avoid adherence. Stood the model for 24 hours until the polymerization was completed.
- F. Removed all stands, spatulas, wax and remained materials with a blade and a rasp. Polished the surface of the model with sandpapers.

#### V. Design and fabrication of abutment tooth:

The average height of a maxillary premolar is 8.5 mm, the mesial-distal width is 7.0 mm and the buccal-palatal width is 9.0 mm. Thus, an 8.0\*8.0\*8.0 mm<sup>3</sup> titanium cube was designed to simulate a premolar metal crown with the mean value as a reference. Computer-Aided Design and Computer-Aided Manufacturing (CAD/CAM) technique was then used to fabricate this abutment tooth in a dental lab after embedding the implant (Fig. 18).



#### VI. Design of model carrier (Fig. 19):

The metal carrier was designed to rotate 360 degrees on the horizontal plane. The vertical plane can switch to 0,  $\pm 15$ ,  $\pm 30$ ,  $\pm 45$  and  $\pm 60$  degrees. The metal clamp, which contacts the model, was 10-mm high. Therefore, the upper two thirds of the model, where the implant located, was without any restriction.

#### VII. Loading equipment and conditions:

- A. Loading machine: Instron 5566 (5560 Series Dual Column System, Instron<sup>®</sup>, MA, USA), the load cell was 5 kg (Fig. 20).
- B. Loading point: considering that the loading component needed to bear a number of experimental impacts, it was made into a cone to increase its structural strength. The loading point, which contacted the abutment tooth, was a circular plane with a radius of 0.5 mm (Fig. 20).
- C. Loading force: 50 N, static load with 30 degrees between loading force and the long axis of the implant (Fig. 22).

#### VIII. Test procedures:

- A. All models were subjected to regression analysis with 0, 10, 20, 30, 40 and 50 N forces, and a positive correlation ( $\gamma > 0.9$ ) was obtained before the formal experiment started.
- B. Given that the four strain gauges were attached at the relatively 180° opposite positions on the implant, one side was tested and recorded first (pressure side, two strain gauges). The pressure side and tension side swapped over by changing the angle of the metal carrier without moving the

model itself. The measured values of the other two strain gauges under pressure were recorded then.

- C. Each strain gauge was tested 6 times with a 7-minute interval between each test to ensure the residual stress from the previous test disappeared. The recorder was zeroed before each experiment.
- D. Once the model and the abutment tooth were placed on the carrier, they were no longer moved. All changes of directions were depended on operating the carrier itself.

#### IX. Output and recording of experimental data:

- A. The potential difference measured by the strain gauge was output to the computer via the signal converter Kyowa PCD 300B (Fig. 21). After calculated by software DCS 100A, the output value was micro-strain. The sampling rate was 10 Hz and the recording time was 20 seconds, starting from the 5 seconds before force loading. A total of 200 output values were recorded. The average of 50 values, taken from the tenth to the fifteenth second, was the MSV of this strain gauge.
- B. The strain gauge recorder remained functioning after the force was removed. Therefore, the recorder showed the micro-strain approaching zero when the residual stress disappeared. The recorder was zeroed before every experiment.

#### X. Analysis of experimental data:

- A. Each implant was tested six times. There were two samples ( $n = 2$ ) for each size of the implant. Therefore, there were twelve sets of data at each grid

position on each size of the implant; i.e. 48 sets of data for each size of the implant. There was a sum of ten different sizes and designs of implants.

- B. There were 192 sets of data in Brånemark group, 288 sets in Astra Tech group; i.e. a total of 480 sets in this experiment.

#### XI. Statistical analysis:

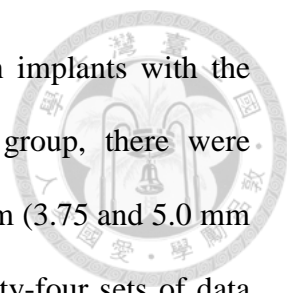
SPSS (Version 19, IBM) was used for statistical analysis. Levene F test was used first for homogeneity test of variance. If the variance was homogeneous, Tukey (HSD) was used for Post-Hoc test; if the variance was not homogeneous, then Games-Howell was used for post-corrected Post-Hoc test.

### **Experiment 2: Comparing the effect of implant diameters and lengths on stress distribution.**

I. to IX.: The fabrication of models and test procedures were the same as experiment 1.

#### X. Analysis of experimental data:

- A. Each implant was tested six times. There were two samples ( $n = 2$ ) for each size of the implant. Therefore, there were twelve sets of data at each grid position on each size of the implant.
- B. Compared the MSV at the grid position of 1.0 mm, the strain gauge closest to the implant platform, on implants with the same diameters but different lengths. There were 24 sets of data to analyse for each group of diameters (Brånemark group: 3.75 and 5.0 mm; Astra Tech group: 4.0S, 5.0S and 5.0 mm); i.e. a total of 120 sets.



C. Compared the MSV at the grid position of 1.0 mm on implants with the same lengths but different diameters. In Brånemark group, there were twenty-four sets of data each in length of 8.5 and 10.0 mm (3.75 and 5.0 mm in diameter); in Astra Tech group, there were also twenty-four sets of data each in 9.0 and 11.0 mm (4.0S and 5.0S in diameter).

#### XI. Statistical analysis:

The method was the same as experiment 1. In addition, the effect of variables, i.e. the diameter and length of the implant, was compared. Multiple regression analysis was used to diagnose collinearity of variables; the correlation coefficient and Condition Index (CI) were observed. The standardized regression coefficient  $\beta$  was used to determine the influence of different variables.

### **Experiment 3: Comparing the effect of implant designs on stress distribution.**

I. to IX.: The fabrication of models and test procedures were the same as experiment 1.

#### X. Analysis of experimental data:

- A. Each implant was tested six times. There were two samples ( $n = 2$ ) for each size of the implant. Therefore, there were twelve sets of data at each grid position on each size of the implant.
- A. Compared the MSV at the grid position of 1.0 mm on Brånemark and Astra Tech implants with similar diameters and lengths; i.e. Brånemark 3.75\*8.5 mm versus Astra Tech 4.0S\*9.0 mm, Brånemark 5.0\*8.5 mm versus Astra



Tech 5.0S\*9.0 mm, Brånemark 3.75\*10.0 mm versus Astra Tech 4.0S\*11.0 mm and Brånemark 5.0\*10.0 mm versus Astra Tech 5.0S\*11.0 mm.

- B. Compared the MSV at the grid position of 1.0 mm on the same length of Astra Tech implants with or without divergence beneath the implant platform; i.e. 4.0S versus 5.0 mm in diameter. The apical diameter of 5.0 implant was 4.0 mm, with an upward and outward divergence at the part under the implant platform, and the diameter increased to 5.0 mm at the top.

XI. Statistical analysis: the method was the same as experiment 1.

## Chapter 5 Results



480 sets of data were generated in this experiment among 10 different sizes and designs of implants, i.e. four types in Brånemark group and six types in Astra Tech group. There were two implants for each type ( $n = 2$ ) with a total of twenty models involved. Each strain gauge was tested six times. Therefore, the MSV was obtained by statistical analysis of twelve sets of data for each strain gauge position on each type of the implant. There were four different vertical heights of strain gauges attached on every implant.

The MSV obtained by all micro-stain gauges in this experiment were negative, showing that the force at the measuring point was mainly compressive.

### Experiment 1

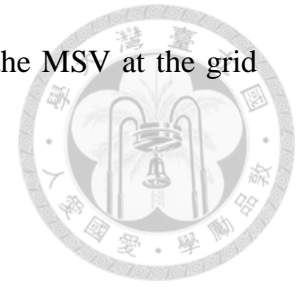
In Brånemark group, the MSV at four different grid positions on each type of implants were shown in Fig. 23 – 26a and Tables 1 – 4. Among all models in this group, the MSV obtained at the grid position of 1.0 mm was the highest, followed by 2.0, 4.0 and 5.0 mm in sequence. The highest MSV in Brånemark group was gained at the grid position of 1.0 mm on the 3.75\*8.5 mm implant. Among all implants, except for the 3.75\*10.0 mm implants, the difference of the MSV between the grid position of 1.0 and 2.0 mm was statistically significant ( $P < 0.05$ ). On the 3.75\*10.0 mm implants, the MSV at the grid position of 2.0 mm was significantly higher than the one at 4.0 mm ( $P < 0.05$ ). A statistically significant difference ( $P < 0.05$ ) of the MSV between the grid position of 4.0 and 5.0 mm was obtained on all sizes of implants. The logarithmic regression analysis showed the correlation between four measurement positions and the

MSV. Their coefficient of determination  $R^2$  was between 0.87 – 0.99; i.e. there was a significant correlation between the grid position and the measured MSV. Moreover, similar results could be obtained from the MSV decreasing rate of the remaining three positions, using the MSV of 1.0 mm as the reference value. The maximum decreasing rate occurred at the grid position of 2.0 mm and the minimum one occurred at 5.0 mm in all models (Fig. 23 – 26b, Table 5).

In Astra Tech group, the MSV at four different grid positions on each implant were shown in Fig. 27 – 32a and Tables 6 – 11. Among all models in this group, the MSV obtained at the grid position of 1.0 mm was the highest, followed by 2.0, 4.0 and 5.0 mm in sequence as found in Brånemark group. The highest MSV in Astra Tech group was obtained at the grid position of 1.0 mm on the 4.0S\*9.0 mm implant. The difference between MSV measured at 1.0 and 2.0 mm on 6 different diameter and length of implants was statistically significant ( $P < 0.05$ ). The same significant difference also occurred between the MSV at 2.0 and 4.0 mm. The logarithmic regression analysis showed the correlation that coefficient of determination  $R^2 > 0.95$  between all grid positions on the implant and the MSV. Similar to Brånemark group, the maximum MSV decreasing rate occurred at the grid position of 2.0 mm and the minimum one was at 5.0 mm in all models of this group (Fig. 27 – 32b, Table 12).

According to above results, the highest MSV occurred at the grid position of 1.0 mm in both Brånemark and Astra Tech groups. The difference achieved statistical significance ( $P < 0.05$ ) on most implants. Therefore, when comparing the strain obtained from

different implants in experiment 2 and 3, the analysis focused on the MSV at the grid position of 1.0 mm.



## Experiment 2

This experiment presented the effect of implant diameters and lengths on stress distribution. The influence of the two variables upon the MSV was compared separately before analysing their influence by multiple regression analysis.

In Brånemark group, the difference of the MSV at the grid position of 1.0 mm on implants with the same diameter but different length was compared (Fig. 33). The results showed that the MSV on 8.5 mm long implants was much higher than the value on 10.0 mm implants. The difference was statistically significant ( $P < 0.05$ ) for both 3.75 mm and 5.0 mm wide implants. The difference of the MSV at the grid position of 1.0 mm on implants with the same length but different diameter was also compared (Fig. 33). Although the MSV on 3.75 mm wide implants was higher than the value on 5.0 mm for both 8.5 and 10.0 mm long implants, only the difference of 8.5 mm group was statistically significant ( $p < 0.05$ ).

The results of multiple regression analysis showed that the correlation coefficient of the diameter and the length was 0.000, CI in 3 dimensions were all less than 10. Therefore, there was no collinearity between these two variables (Table 13). Using diameter as a factor to process linear regression analysis, the standardised coefficient  $\beta$  (i.e. the correlation coefficient) was -0.519 with significance ( $P < 0.05$ ) and the corrected  $R^2$  (i.e.

variable explanatory power) was 0.253. Using length as another factor, the correlation coefficient was 0.677 with significance ( $P < 0.05$ ) and the variable explanatory power was 0.446 (Table 14). Therefore, both the length and the diameter were significantly related to the MSV in Brånemark group. Moreover, the effect of the length was greater than the diameter.

In Astra Tech group, implants with the same design, i.e. diameter 4.0S and 5.0S, were used for comparison in order to reduce the error caused by the design (diameter 5.0 mm). The difference of the MSV at the grid position of 1.0 mm on implants with the same diameter but different length was shown in Fig. 34. The MSV on 9.0 mm long implants was much higher than the value on 11.0 mm implants. The difference was statistically significant ( $P < 0.05$ ) for both 4.0S and 5.0S groups. Similar comparison on implants with the same length but different diameter showed that the MSV of diameter 4.0S implants was significant higher than 5.0S implants ( $P < 0.05$ ) in both 9.0 and 11.0 mm groups (Fig. 34).

The results of multiple regression analysis showed that the correlation coefficient of the diameter and the length was 0.000, CI in 3 dimensions were all less than 10. Therefore, there was no collinearity between these two variables (Table 15). Using diameter as a factor to process linear regression analysis, the standardised coefficient  $\beta$  (i.e. the correlation coefficient) was -0.726 with significance ( $P < 0.05$ ) and the corrected  $R^2$  (i.e. variable explanatory power) was 0.521. Using length as another factor, the correlation coefficient was 0.456 with significance ( $P < 0.05$ ) and the variable explanatory power was 0.196 (Table 16). Therefore, both the length and the diameter were significantly

related to the MSV in Astra Tech group. The effect of the diameter was greater than the length.

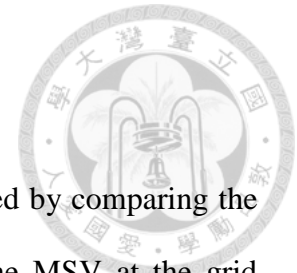


### **Experiment 3**

The comparison of the MSV at the grid position of 1.0 mm for Brånemark and Astra Tech implants with similar diameter and length was shown in Table 35. The MSV of Brånemark 3.75\*8.5 mm implants was higher than the MSV of Astra Tech 4.0S\*9.0 mm implants. The MSV of Brånemark 5.0\*8.5 mm implants was higher than the MSV of Astra Tech 5.0S\*9.0 mm implants. The MSV of Brånemark 5.0\*10.0 mm implants was higher than the MSV of Astra Tech 5.0S\*11.0 mm implants. The differences of these three groups were all statistically significant ( $P < 0.05$ ). The MSV of Brånemark 3.75\*10.0 mm implants was lower than the MSV of Astra Tech 4.0S\*11.0 mm implants. However, the difference between the two values was not statistically significant ( $P < 0.05$ ).

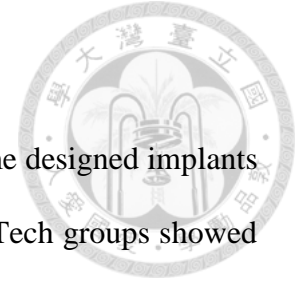
Astra Tech implants in diameter 4.0S and 5.0 mm were chosen to analyse the effect of the outward design and increased surface area under the implant platform on stress distribution. The MSV at the grid position of 1.0 mm was shown in Table 36. Regardless of the length of implants, the MSV of diameter 4.0S implants was significantly higher than the MSV of 5.0 mm implants ( $P < 0.05$ ).

## Chapter 6 Discussion



In experiment 1, the range of primary supporting area was evaluated by comparing the MSV at four different vertical positions on the same implant. The MSV at the grid position of 1.0 mm was higher than values at other three positions in both Brånemark and Astra Tech groups. The results were statistically significant ( $P < 0.05$ ), except for Brånemark 3.75\*10.0 mm group. The MSV at the grid position of 2.0 mm was significantly higher than the values at 4.0 mm ( $P < 0.05$ ), except for Brånemark 3.75\*8.5 mm group. Besides, there was a significant correlation between the four positions and the MSV via logarithmic regression analysis. The coefficient of determination  $R^2 > 0.87$  and the correlation coefficient  $R > 0.9$ . The MSV at the grid position of 4.0 mm was even 71% – 81% lower than the value at 1.0 mm in Brånemark group. The Astra Tech group showed a greater variance of decreased MSV (37% – 88%), but the maximum decreasing rate was still within 2.0 mm. Therefore, the range of 2.0 mm below the implant platform was the main area for implants to distribute stress and could be defined as the range of primary supporting area.

The result of this experiment proved that “the stress distributed by each position of the implant is not equal.” It matched the conclusion of Rieger et al. (1990) and Bidez and Misch (1992) by FEM and photoelastic analysis: the crestal zone has the greatest impact upon stress distribution when the implant is under loading, and the implant cervical area has the maximum stress concentration. It also matched the result of Schrotenboer et al. (2008) that stress concentrates at the top of the crestal bone, regardless of implant designs.

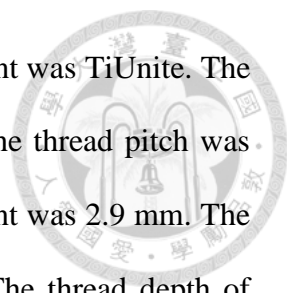


In experiment 2, the effect of the diameter and the length on the same designed implants upon stress distribution was discussed. Both Brånemark and Astra Tech groups showed that the implant diameter and length had significant effect on the MSV. There was no collinearity between these two factors. However, an opposite result of the variable explanatory power was obtained by multiple regression analysis. In Brånemark group, the influence of the diameter was lesser than the length. This could be speculated from the result that the MSV of 3.75 mm wide implants was higher than the value of 5.0 mm implants. However, statistical significance ( $P < 0.05$ ) was only achieved in the 8.5 mm long group. In Astra Tech group, the influence of the diameter was greater than the length. All differences between these two variables among each group were statistically significant ( $P < 0.05$ ).

Himmlová et al. (2004) used 3D FEM to compare the effect of the implant diameter and length on the implant neck stress. They found that the increase of implant diameter, compared with the length, had greater impact upon decreasing stress around the implant neck. The same conclusion was obtained in Astra Tech group, but not in Brånemark group. In addition to some inevitable errors in the experiment, the main factor was too small the number of samples. There were only two samples per implant. Therefore, the effect of each sample on the whole was increased. If the subsequent sample could be expanded for the analysis of influence, the result may be more reliable.

In experiment 3, the effect of different implant designs upon stress distribution was compared. The implants used in Brånemark group were MK III TiUnite® system with





double-helix thread and parallel wall design. The surface management was TiUnite. The thread depth of diameter 3.75 mm (RP) implants was 0.32 mm. The thread pitch was 0.6 mm. The thread lead was 1.2 mm. The tip diameter of the implant was 2.9 mm. The collar height was 0.8 mm, and the collar diameter was 4.1 mm. The thread depth of diameter 5.0 mm (WP) implants was 0.425 mm. The thread pitch was 0.8 mm. The thread lead was 1.6 mm. The tip diameter of the implant was 3.8 mm. The collar height was 0.8 mm, and the collar diameter was 5.1 mm.

The implants used in Astra Tech group were OsseoSpeed system with the surface management of TiOblast. The titanium dioxide particles were sprayed on the implant surface with the design of microthreads at the crestal module. The macrothread depth was 0.3 mm. The thread pitch was 0.66 mm, and the collar height was 0.32 mm. The range of microthreads on the straight designed implants (i.e. diameter 4.0S and 5.0 S) was 3.5 mm. The range on the outward designed implants (i.e. diameter 5.0 mm) was 5.5 mm. The microthreads were triple-helix threads with the thread pitch of 0.2 mm and the thread lead of 0.66 mm. The thread pitch was the same as the macrothreads. The diameter of the platform on the outward designed implants was 5.0 mm with the tip diameter of 4.0 mm.

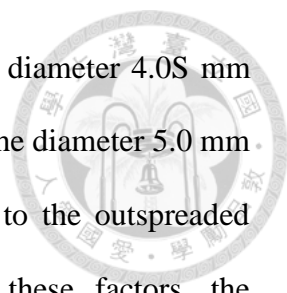
Schrotenboer et al. (2008) used 2D FEM and found that the design of microthreads, compared with the smooth designed implant neck, increased the stress at the crestal area under loading. Palmer et al. (2000) also proved that implants with retentive elements at the neck could maintain the height of the marginal bone. In addition, Abrahamsson and Berglundh (2006) observed implants placed 10 months in dogs and found that the bone-

implant contact rate in the microthreads group was 81.8%, compared with 72.8% in the group without microthreads.



In this experiment, comparing Brånemark and Astra Tech implants with similar diameter and length, the groups with significant difference ( $P < 0.05$ ) had higher MSV on slightly narrower and shorter implants; i.e. the effect of the diameter and the length proved in experiment 2 was also obvious among different designed implants. The only exception was Brånemark 3.75\*10.0 implants which had lower MSV than Astra Tech 4.0S\*11.0 implants. The result of this group may be affected by other factors, such as different designs. However, the difference in this group was not significant. Therefore, the effect of the implant design may be lesser than the effect of the diameter or the length upon stress distribution.

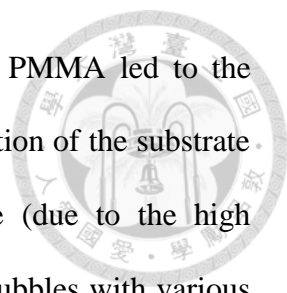
In Astra Tech group, the effect of implant designs upon the MSV was compared. The MSV of the 5.0 mm implants, which had an outward design under the platform, was significantly higher ( $P < 0.05$ ) than the MSV of the 4.0S mm implants (straight form). The same result was gained in both 9.0 and 11.0 mm groups. However, there were some controversial issues to consider. First, the component and direction of the loading force at the outspreaded part must be different from a cylinder implant, even though the same force magnitude and angle were given. In addition, to paste the strain gauge on a smooth surface, the threads on the implant surface were coated by PMMA resin and the implant turned into a cylinder. However, this led to variant distances between each strain gauge and the surface of the outspreaded designed implants. In other words, the more apical strain gauge had a further distance to the implant surface. Besides, the



ranges of microthreads on the two implants were different. On the diameter 4.0S mm implants, the range was 3.5 mm. The range increased to 5.5 mm on the diameter 5.0 mm implants. The increased diameter (from 4.0 mm to 5.0 mm) due to the outspreaded design may also contribute to stress distribution. Because of these factors, the contribution of the outspreaded design to stress dispersion must be carefully evaluated and interpreted.

Some basic causes of the experiment errors, including inevitable errors of instruments and model fabrication, were discussed in the next part.

The embedding material used in this experiment was polymethylmethacrylate (PMMA). This was because the elasticity coefficient of human cancellous bone is between 0.65 – 9.5 GPa and the elasticity coefficient of self-cured PMMA is between 1.8 – 3.1 GPa. According to the research by El-Homsi et al. (2004), the characteristics of PMMA could be used as an embedding material to simulate the cancellous bone for *in vitro* experiments of dental implants, especially for the maxillary edentulous area with low bone density. Its strength was also sufficient for long-term test. Heat-cured resin created an obvious gap around the implant after polymerisation. Therefore, PMMA was a common choice for experiments to fabricate models and simulate the cancellous bone (Cehreli et al., 2004; Akca et al., 2002, 2008; Yang et al., 2011).



Nevertheless, the porosity occurred during the process of mixing PMMA led to the change of its physical characteristics. Even with the accurate proportion of the substrate to the catalyst (powder and liquid), the longer the mixing time (due to the high viscosity), the more air would be mixed into the resin and caused bubbles with various sizes. These bubbles could not be discharged completely even after shaking on a vibrator and caused porosity after polymerisation. On the contrary, if the mixing time was insufficient, the characteristics of resin may be changed due to incomplete polymerisation in spite of the decreased chance of producing bubbles. In the process of this experiment, the model mode was placed on a vibrator to shake and eliminate more bubbles. The model in the polymerisation process was then placed in a pressure cooker to suppress the generation of bubbles by pressure. The models of this experiment were numerous, and the mixing procedure was limited by PMMA characters of short working time and high viscosity. Only one model could be produced per time, instead of a one-time unified mixture of PMMA resin. The difference of physical characteristics between each model due to the process of polymerisation was uncountable and may affect the output value of micro-strain gauges.

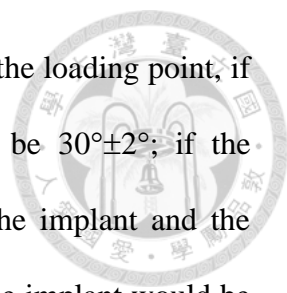
Moreover, the pasted angle and position of the micro-strain gauge had a certain impact upon the difference of values among models. In order to increase the precision of positions, every implant in this experiment was put on the same scaled table to paste the strain gauges. It was still impossible to make every strain gauge pasted on exactly the same position due to the permissible limit. Besides, to ensure the adhesive was completely functional and to avoid any dislodgement during the process of resin polymerisation or force loading, it was necessary to place the strain gauge-pasted implants 24 hours before doing the next step.



Given that the length of the implant in this experiment was between 8.5 – 11.0 mm and the diameter was between 3.75 – 5.0 mm, the surface area of an implant was limited. The base length of a micro-strain gauge was 3.0 mm. Therefore, there was a maximum of two strain gauges pasted on one vertical plane. To solve this problem, the metal stage was designed to rotate on the vertical plane so the four strain gauges on the same implant, which were at opposite 180°, could undergo pressure experiments without moving the model and decrease errors caused by moving.

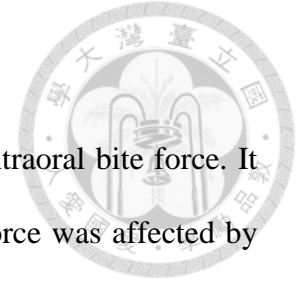
Furthermore, when considering about the direction of the force loaded on the implant, the anatomical factors of maxilla and mandible cause the difficulty of surgical placement. It is hard to let the force passes through the long axis of the inserted root-form implant. Bone undercuts due to long-term missing teeth obstruct the placement of implants and affect the direction of force loaded. When the chewing behavior occurs, in addition to the vertical bite force between upper and lower dentitions (apical force, occlusal force), lateral force from various directions is also produced during the process of grinding food. This includes facial force, lingual force, mesial force and distal force. Therefore, not only the vertical force but also other different directions should be considered when it comes to the force experiment (Misch, 2004).

ISO (International Organization for Standardization) proposed a suggested experimental device for the dynamic fatigue experiment of intradermal dental implants (Fig. 37). The loading instrument needed to be accurate and repeatable and there was no lateral



constraint in the process of force loading. With a clear definition of the loading point, if the connector was straight, the suggested angle of force would be  $30^{\circ} \pm 2^{\circ}$ ; if the connector was angular, and the angle between the long axes of the implant and the connector was  $\alpha$ , the angle between the force and the long axis of the implant would be  $\alpha + 10^{\circ}$  ( $+2^{\circ}/-1^{\circ}$ ). All of the environmental settings in the experiment were under the most unfavorable conditions (ISO 14801, 2007).

In this experiment, the rotation of the metal stage was used to set the direction of the force to  $30^{\circ}$ . However, there might be some angular errors among the model, the metallic device and the dynamic loading machine. These included the tightness of every fixation screw on the metal clamp, the angle that the clamps fixed, the vertical relationship between the force-receiving surface of the abutment tooth and the force-loading arm, and different positions that the loading point hit the abutment surface on different models. Any of these errors may cause the force and the micro-strain gauges not on the same straight line and increase the variance among models. To reduce artificial errors, the abutment tooth was fabricated by CAD/CAM technique. There was a mark of the stress point on each abutment tooth. However, due to different types of implants, it was unavailable to use the same abutment tooth on every model. Thus, minor error of the marking point was possible. Even with the same abutment tooth, it was still very difficult for the loading point to hit on the stress point accurately every time. Furthermore, the metal stage was designed to rotate on the vertical plane, and the rotation angle was set to  $15^{\circ}$  per scale when the stage was produced. But a minor angular error may still occur during the process of angle fixation.

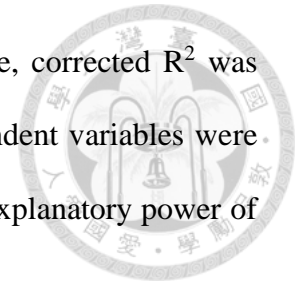


The magnitude of the force in this experiment was related to the intraoral bite force. It was generally believed that during the chewing process, the bite force was affected by central control mechanisms and the sensory feedback of peripheral mechanoreceptors (Van Der Bilt et al., 2010). The food bolus was cut and grinded smoothly and efficiently before being swallowed (Peyron et al., 2004). In earlier studies, despite many different devices were used to measure bite force, they were not suitable for recording during the chewing process. These devices increased the occlusal vertical dimension and caused obstacles of cheek, lips and tongue movement (Kohyama et al., 2004; Shimada et al., 2008).

Due to the improvement of research methods, it was currently possible to record the dynamic bite force during the chewing process, via the intraoral strain gauge. Shimada et al. (2012) put the intraoral strain gauges on the first molars of subjects and tested the bite force of five different kinds of foods (carrots, cookies, crackers, cheese and chewing gum). The result showed that all bite forces were under 35N (Fig. 38). According to the above reasons, the force in this experiment was set to a 50N static force and applied by Instron 5566. This machine could apply repeatedly accurate force and its accuracy was to the fourth digit after the decimal point.

This experiment used a total of 10 different diameter, length and design of implants, but there were only two implants for each type. This led to the problem of insufficient sample number. In the statistical analysis, the variable explanatory power  $R^2$  was affected by the size of the sample and showed overestimation. Moreover, the smaller the

sample was, the more prone the overestimation showed. Therefore, corrected  $R^2$  was used. The amount of error variance and the total variance of dependent variables were both divided by degree of freedom to avoid overestimation of the explanatory power of the entire regression model due to the too small sample.



Considering the application of these results to clinical conditions, it must be noted that the model was a homogeneous material and ignored the presence of cortical bone, despite the elasticity coefficient of PMMA model was similar to cancellous bone. The reason was that multifactor increased the difficulty of model fabrication and data analysis. Thus, the simplified strategy was taken and did not stand for the real alveolar bone environment. Therefore, although the results of such *in vitro* experiments had practical significance, their clinical application still needed to be cautious.

The range of primary supporting area was further defined as within 2.0 mm beneath the implant platform in this condition-limited experiment. The results proved that the implant diameter, length and design all had impact upon stress distribution at implant-bone contact. For further research, more various experimental methods should be used to cross-compare the results in this experiment, clearly identify the range of the main stress area, and study more details about the difference of implant designs at this area. With a view to the maximum use of primary supporting area, this experiment is only an initial start. More data are needed for further results.



## Chapter 7 Conclusion



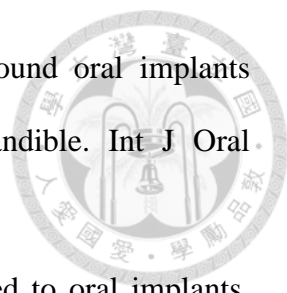
In conclusion, the proposed experiment proved that the range of primary supporting area, which had the maximum stress concentration, was within 2.0 mm under the implant platform. Moreover, both the implant diameter and the length affected the MSV at primary supporting area significantly. These results not only defined more details about the range of primary supporting area but also proved the factors that should be considered when it came to stress distribution of implants.

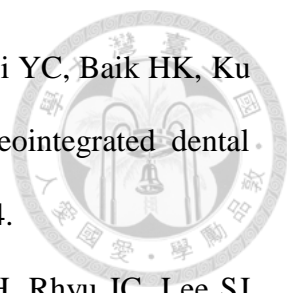
This experiment was just an initial study about the characteristics of primary supporting area. Studying this area is important for implant design and clinical judgment. Therefore, further research is needed to find out the most efficient design to disperse stress and improve the implant success rate, especially for poor quality and quantity bone.

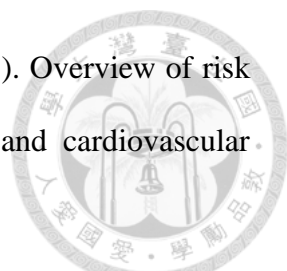
## Reference

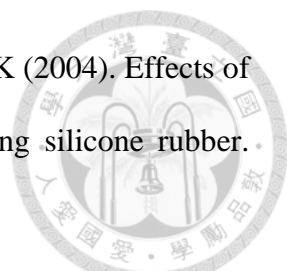


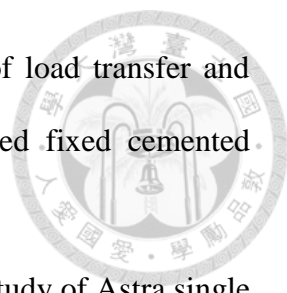
1. Abduo J, Swain M (2012). Influence of vertical misfit of titanium and zirconia frameworks on peri-implant strain. *Int J Oral Maxillofac Implants* 27:529-536.
2. Abrahamsson I, Berglundh T (2006). Tissue characteristics at microthreaded implants: an experimental study in dogs. *Clin Implant Dent Relat Res* 8:107-113.
3. Abuhussein H, Pagni G, Rebaudi A, Wang HL (2010). The effect of thread pattern upon implant osseointegration. *Clin Oral Implants Res* 21:129-136.
4. Adell R, Lekholm U, Rockler B, Brånemark PI (1981). A 15-year study of osseointegrated implants in the treatment of the edentulous jaw. *Int J Oral Surg* 10:387-416.
5. Adell R, Eriksson B, Lekholm U, Brånemark PI, Jemt T (1990). Long-term follow-up study of osseointegrated implants in the treatment of totally edentulous jaws. *Int J Oral Maxillofac Implants* 5:347-359.
6. Akca K, Cehreli MC, Iplikcioglu H (2002). A comparison of three-dimensional finite element stress analysis with in vitro strain gauge measurements on dental implants. *Int J Prosthodont* 15:115-121.
7. Akca K, Cehreli MC (2008). A photoelastic and strain gauge analysis of interface force transmission of internal-cone implants. *Int J Periodontics Restorative Dent* 28:391-399.
8. Albrektsson T, Brånemark PI, Hansson HA, Lindström J (1981). Osseointegrated titanium implants. Requirements for ensuring a long-lasting, direct bone-to-implant anchorage in man. *Acta Orthop Scand* 52:155-170.
9. Artzi Z, Carmeli G, Kozlovsky A (2006). A distinguishable observation between survival and success rate outcome of hydroxyapatite-coated implants in 5–10 years in function. *Clin Oral Implants Res* 17:85-93.

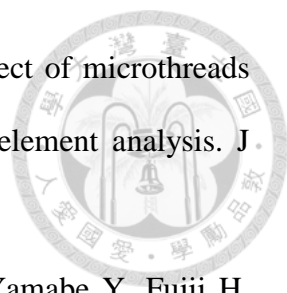
- 
10. Barbier L, Schepers E (1997). Adaptive bone remodeling around oral implants under axial and nonaxial loading conditions in the dog mandible. *Int J Oral Maxillofac Implants* 12:215-223.
  11. Bidez MW, Misch CE (1992). Issues in bone mechanics related to oral implants. *Implant Dent* 1:289-294.
  12. Binon PP (2000). Implants and components. *Int J Oral Maxillofac Implants* 15:76-94.
  13. Bozkaya D, Muftu S, Muftu A (2004). Evaluation of load transfer characteristics of five different implants in compact bone at different load levels by finite elements analysis. *J Prosthet Dent* 92:523-530.
  14. Brighton CT, Schaffer JL, Shapiro DB, Tang JJ, Clark CC (1991). Proliferation and macromolecular synthesis by rat calvarial bone cells grown in various oxygen tensions. *J Orthop Res* 9:847-854.
  15. Bumgardner JD, Boring JG, Cooper RC Jr, Gao C, Givaruangsawat S, Gilbert JA, Misch CM, Steflik DE (2000). Preliminary evaluation of a new dental implant design in canine models. *Implant Dent* 9:252-260.
  16. Buser D, Mericske-Stern R, Bernard JP, Behneke A, Behneke N, Hirt HP, Belser UC, Lang NP (1997). Long-term evaluation of non-submerged ITI implants. Part 1: 8-year life table analysis of a prospective multi-center study with 2359 implants. *Clin Oral Implants Res* 8:161-172.
  17. Carlsson LV, Alberktsson T, Berman C (1989). Bone response to plasma-cleaned titanium implants. *Int J Oral Maxillofac Implants* 4:199.
  18. Cehreli M, Duyck J, De Cooman M, Puers R, Naert I (2004). Implant design and interface force transfer. A photoelastic and strain-gauge analysis. *Clin Oral Implants Res* 15:249-257.

- 
19. Chun HJ, Cheong SY, Han JH, Heo SJ, Chung JP, Rhyu IC, Choi YC, Baik HK, Ku Y, Kim MH (2002). Evaluation of design parameters of osseointegrated dental implants using finite element analysis. *J Oral Rehabil* 29:565-574.
20. Chung S, Heo SJ, Koak JY, Kim SK, Lee JB, Han JS, Han CH, Rhyu IC, Lee SJ (2008). Effects of implant geometry and surface treatment on osseointegration after functional loading: a dog study. *J Oral Rehabil* 35:229-236.
21. Cooper LF (2000). A role for surface topography in creating and maintaining bone at titanium endosseous implants. *J Prosthet Dent* 84:522-534.
22. Cowin SC (1989). *Bone mechanics*.
23. Cowin SC, Mehrabadi MM (1989). Identification of the elastic symmetry of bone and other materials. *J Biomech* 22:503-515.
24. Cowin SC, Moss-Salentijn L, Moss ML (1991). Candidates for the mechanosensory system in bone. *J Biomech Eng* 113:191-197.
25. Duyck J, Rønold HJ, Van Oosterwyck H, Naert I, Vander Sloten J, Ellingsen JE (2001). The influence of static and dynamic loading on marginal bone reactions around osseointegrated implants: an animal experimental study. *Clin Oral Implants Res* 12:207-218.
26. El-Homsi F, Lockowandt P, Linden LA (2004). Simulating periodontal effects in dental osseointegrated implants: effect of an intramobile damping element on the fatigue strength of dental implants--an in vitro test method. *Quintessence Int* 35:449-455.
27. Frost H (1987). The mechanostat: a proposed pathogenetic mechanism of osteoporosis and bone mass effects of mechanical and nonmechanical agents. *Bone Miner* 2:73-85.

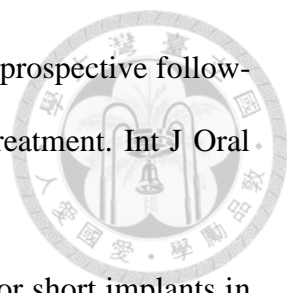
- 
28. Genco R, Glurich I, Haraszthy V, Zambon J, DeNardin E (2001). Overview of risk factors for periodontal disease and implications for diabetes and cardiovascular disease. *Compend Contin Educ Dent* 22:21-23.
29. Geng J, Ma QS, Xu W, Tan KB, Liu GR (2004). Finite element analysis of four thread-form configurations in a stepped screw implant. *J Oral Rehabil* 31:233-239.
30. Gotfredsen K (2012). A 10-year prospective study of single tooth implants placed in the anterior maxilla. *Clin Implant Dent Relat Res* 14:80-87.
31. Himmlova L, Dostálová T, Kácovský A, Konvicková S (2004). Influence of implant length and diameter on stress distribution: a finite element analysis. *J Prosthet Dent* 91:20-25.
32. Hoshaw SJ, Brunski JB, Cochran GV (1994). Mechanical loading of Branemark implants affects interfacial bone modeling and remodeling. *Int J Oral Maxillofac Implants* 9:345-360.
33. Isidor F (2006). Influence of forces on peri-implant bone. *Clin Oral Implants Res* 17:8-18.
34. ISO 14801 (2007). *Dentistry — Implants — Dynamic fatigue test for endosseous dental implants.*
35. Karoussis IK, Brägger U, Salvi GE, Bürgin W, Lang NP (2004). Effect of implant design on survival and success rates of titanium oral implants: a 10-year prospective cohort study of the ITI Dental Implant System. *Clin Oral Implants Res* 15:8-17.
36. Kawara M, Komiyama O, Kimoto S, Kobayashi N, Kobayashi K, Nemoto K (1998). Distortion behavior of heat-activated acrylic denture-base resin in conventional and long, low-temperature processing methods. *J Dent Res* 77:1446-1453.
37. Kim E (2005). *Dental Implant Prosthetics.* *J Prosthodont* 14:212-214.

- 
38. Kohyama K, Hatakeyama E, Sasaki T, Dan H, Azuma T, Karita K (2004). Effects of sample hardness on human chewing force: a model study using silicone rubber. *Arch Oral Biol* 49:805-816.
39. Kong L, Liu BL, Hu KJ, Li DH, Song YL, Ma P, Yang J (2006). Optimized thread pitch design and stress analysis of the cylinder screwed dental implant. *Hua Xi Kou Qiang Yi Xue Za Zhi* 24:509-512, 515.
40. Lee DW, Choi YS, Park KH, Kim CS, Moon IS (2007). Effect of microthread on the maintenance of marginal bone level: a 3-year prospective study. *Clin Oral Implants Res* 18:465-470.
41. Ma P, Liu HC, Li DH, Lin S, Shi Z, Peng QJ (2007). Influence of helix angle and density on primary stability of immediately loaded dental implants: three-dimensional finite element analysis. *Zhonghua Kou Qiang Yi Xue Za Zhi* 42:618-621.
42. Misch CE (1990). Density of bone: effect on treatment plans, surgical approach, healing, and progressive boen loading. *Int J Oral Implantol* 6:23-31.
43. Misch CE, Bidez M (1994). Implant-protected occlusion: a biomechanical rationale. *Compendium* 15:1330-1344.
44. Misch CE (2004). *Dental implant prosthetics*. St Louis: Mosby.
45. Misch CE (2008). *Contemporary implant dentistry*. 3rd ed. St Louis: Mosby.
46. Motoyoshi M, Yano S, Tsuruoka T, Shimizu N (2005). Biomechanical effect of abutment on stability of orthodontic mini-implant. *Clin Oral Implants Res* 16:480-485.
47. Nicolella DP, Lankford J, Jepsen KJ, Davy DT (1997). Correlation of physical damage development with microstructure and strain localization in bone. *ASME* 35:311-312.

- 
48. Nissan J, Ghelfan O, Gross M, Chaushu G (2010). Analysis of load transfer and stress distribution by splinted and unsplinted implant-supported fixed cemented restorations. *J Oral Rehabil* 37:658-662.
49. Palmer RM, Palmer PJ, Smith BJ (2000). A 5-year prospective study of Astra single tooth implants. *Clin Oral Implants Res* 11:179-182.
50. Peyron MA, Mishellany A, Woda A (2004). Particle size distribution of food boluses after mastication of six natural foods. *J Dent Res* 83:578-582.
51. Pierrisnard L, Renouard F, Renault P, Barquins M (2003). Influence of implant length and bicortical anchorage on implant stress distribution. *Clin Implant Dent Relat Res* 5:254-262.
52. Pilliar R, Deporter DA, Watson PA, Valiquette N (1991). Dental implant design—effect on bone remodeling. *J Biomed Mater Res* 25:467-483.
53. Rieger MR, Fareed K, Adams WK, Tanquist RA (1989). Bone stress distribution for three endosseous implants. *J Prosthet Dent* 61:223-228.
54. Rieger M, Mayberry M, Brose M (1990). Finite element analysis of six endosseous implants. *J Prosthet Dent* 63:671-676.
55. Roberts WE, Smith RK, Zilberman Y, Mozsary PG, Smith RS (1984). Osseous adaptation to continuous loading of rigid endosseous implants. *Am J Orthod* 86:95-111.
56. Rubin CT, Hausman M (1988). The cellular basis of Wolff's law. Transduction of physical stimuli to skeletal adaptation. *Rheum Dis Clin North Am* 14:503-517.
57. Sachs F (1988). Mechanical transduction in biological systems. *Crit Rev Biomed En* 16:141-169.
58. Sachs F (1991). Mechanical transduction by membrane ion channels: a mini review. *Mol Cell Biochem* 104:57-60.

- 
59. Schrottenboer J, Tsao YP, Kinariwala V, Wang HL (2008). Effect of microthreads and platform switching on crestal bone stress levels: a finite element analysis. *J Periodontol* 79:2166-2172.
60. Shimada A, Tanaka M, Yamashita R, Noguchi K, Torisu T, Yamabe Y, Fujii H, Murata H (2008). Automatic regulation of occlusal force because of hardness-change of the bite object. *J Oral Rehabil* 35:12-9.
61. Shimada A, Yamabe Y, Torisu T, Baad-Hansen L, Murata H, Svensson P (2012). Measurement of dynamic bite force during mastication. *J Oral Rehabil* 39:349-356.
62. Siegele, D, Soltesz U (1989). Numerical investigations of the influence of implant shape on stress distribution in the jaw bone. *Int J Oral Maxillofac Implants* 4:333-340.
63. Steigenga J, Al-Shammari K, Misch C, Nociti FH Jr, Wang HL (2004). Effects of implant thread geometry on percentage of osseointegration and resistance to reverse torque in the tibia of rabbits. *J Periodontol* 75:1233-1241.
64. Tada S, Stegaroiu R, Kitamura E, Miyakawa O, Kusakari H (2003). Influence of implant design and bone quality on stress/strain distribution in bone around implants: a 3-dimensional finite element analysis. *Int J Oral Maxillofac Implants* 18:357-368.
65. Tonetti MS, Schmid J (1994). Pathogenesis of implant failures. *Periodontol* 2000 4:127-138.
66. Tonetti MS (1998). Risk factors for osseodisintegration. *Periodontol* 2000 17:55-62.
67. Vaillancourt H, Pilliar R, McCammond D (1995). Finite element analysis of crestalbone loss around porous-coated dental implants. *J Appl Biomater* 6:267-282.
68. Van der Bilt A, Pocztaruk RL, Frasca LC, van der Glas HW, Abbink JH (2011). The influence of auditory and visual information on the neuromuscular control of chewing crispy food. *Eur J Oral Sci* 119:427-434.



- 
69. Weibrich G, Buch RS, Wegener J, Wagner W (2001). Five-year prospective follow-up report of the Astra tech standard dental implant in clinical treatment. *Int J Oral Maxillofac Implants* 16:557-562.
70. Yang TC, Maeda Y, Gonda T (2011). Biomechanical rationale for short implants in splinted restorations: an in vitro study. *Int J Prosthodont* 24:130-132.
71. Zarb GA, Alberktsson T (1990). Criteria for determining clinical success with osseointegrated dental implants. *Cah prothese* 71:19-26.
72. Zarb GA, Schmitt A (1990a). The longitudinal clinical effectiveness of osseointegrated dental implants: the Toronto study. Part I: Surgical results. *J Prosthet Dent* 63:451-457.
73. Zarb GA, Schmitt A (1990b). The longitudinal clinical effectiveness of osseointegrated dental implants: the Toronto Study. Part II: The prosthetic results. *J Prosthet Dent* 64:53-61.
74. Zarb GA, Schmitt A (1990c). The longitudinal clinical effectiveness of osseointegrated dental implants: the Toronto study. Part III: Problems and complications encountered. *J Prosthet Dent* 64:185-194.

# Figures

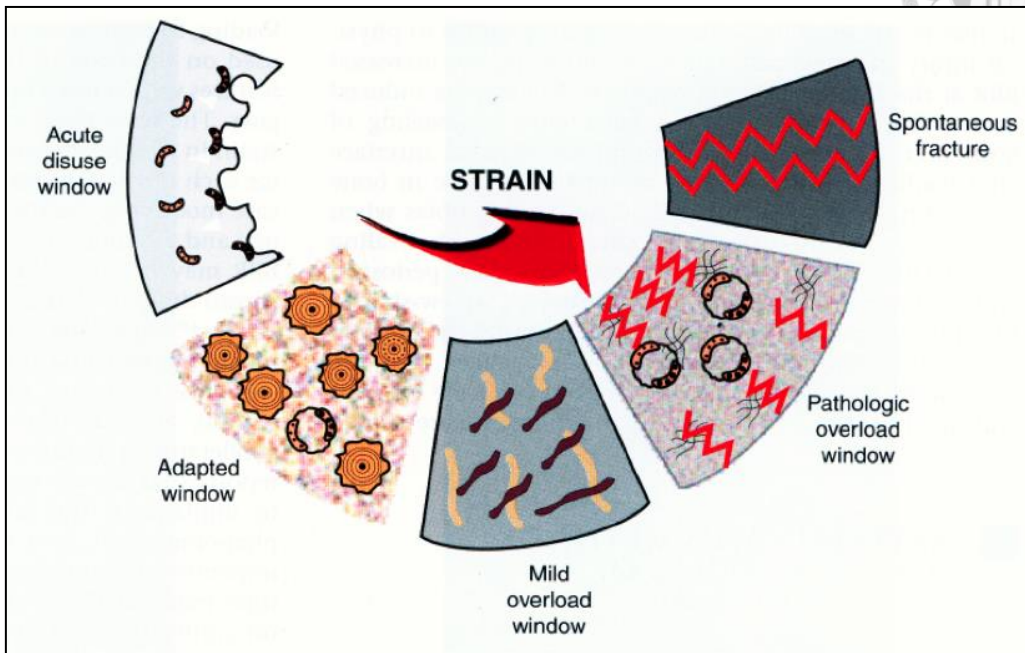


Fig. 1: Diagram of Mechanostat theory.

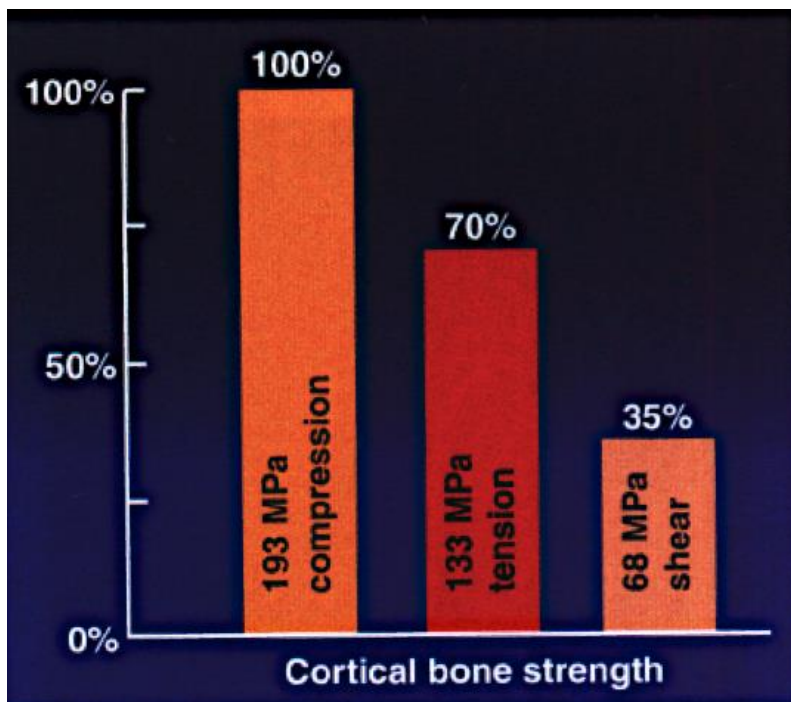


Fig. 2: Cortical bone has different intensity of response to three various forces.

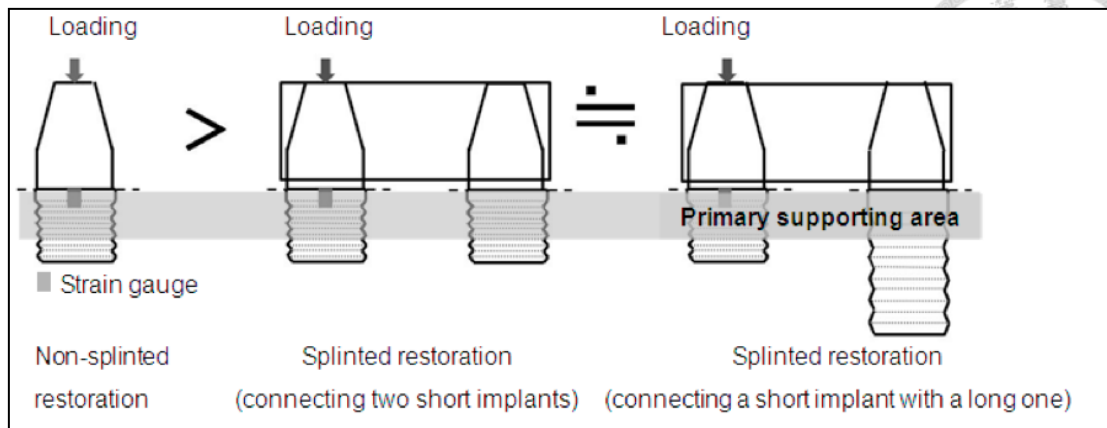


Fig. 3: Yang et al. (2001) proposed the concept of primary supporting area and suggested that the part beyond this area does not have much impact upon stress distribution.

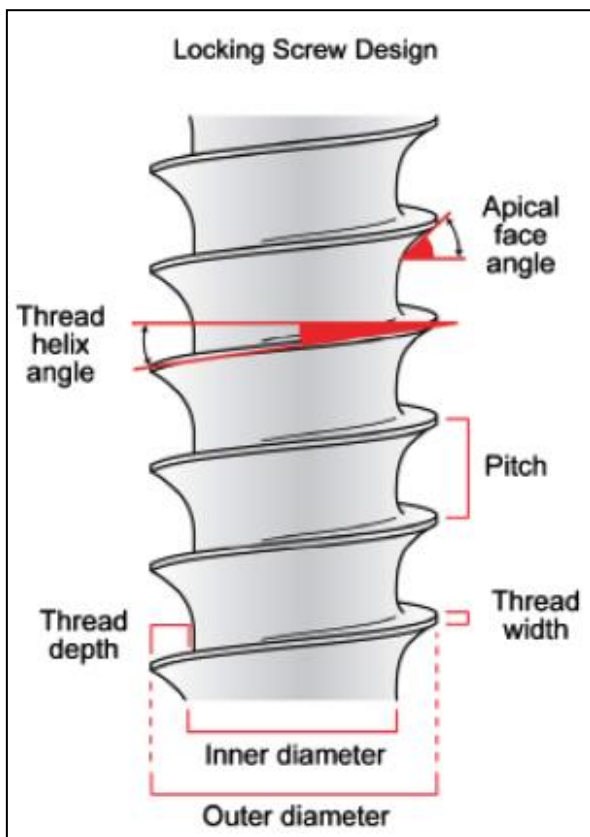


Fig. 4: The basic macrothread structures of dental implants (Abuhussein et al., 2012).



(a)

(b)

(c)

Fig. 5: The structural diagrams of implants in this experiment: (a) Brånemark MK III TiUnite 3.75 mm; (b) Astra Tech OsseoSpeed 5.0 mm; (c) Astra Tech OsseoSpeed 5.0S mm.

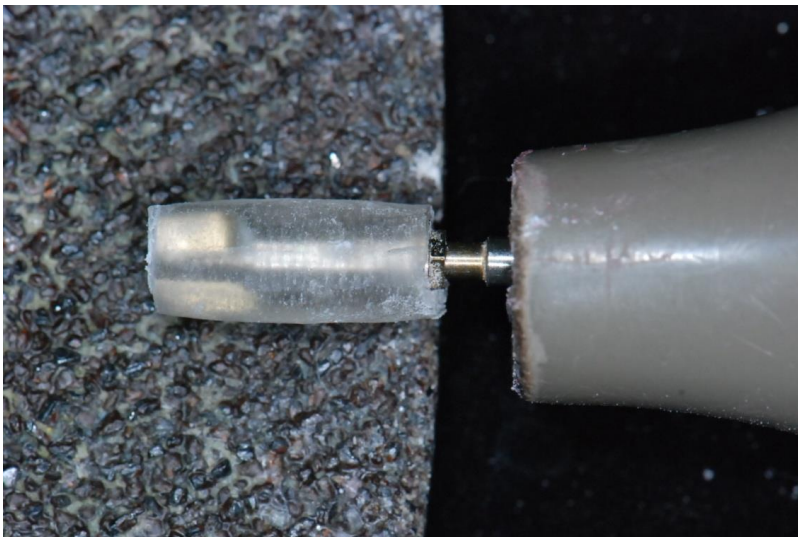


Fig. 6: Connect the implant with the metal axis of the impression coping and put the axis into a mechanical hand piece as a bur axis. Put a rasp beneath the implant and remove excess PMMA resin.



Fig. 7: Brånemark implant covered with resin after polishing.



Fig. 8: Astra Tech implant covered with resin after polishing.

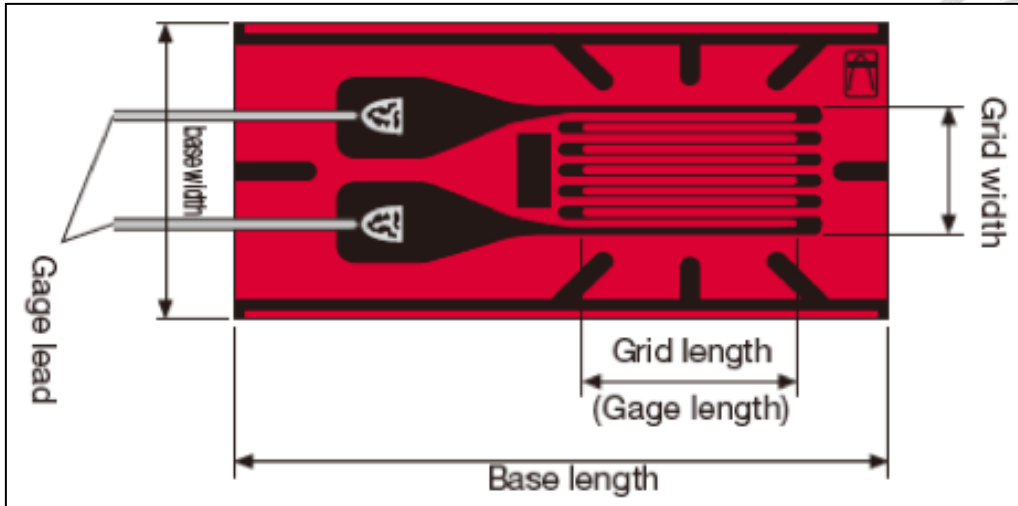


Fig. 9: Diagram of micro-strain gauge.

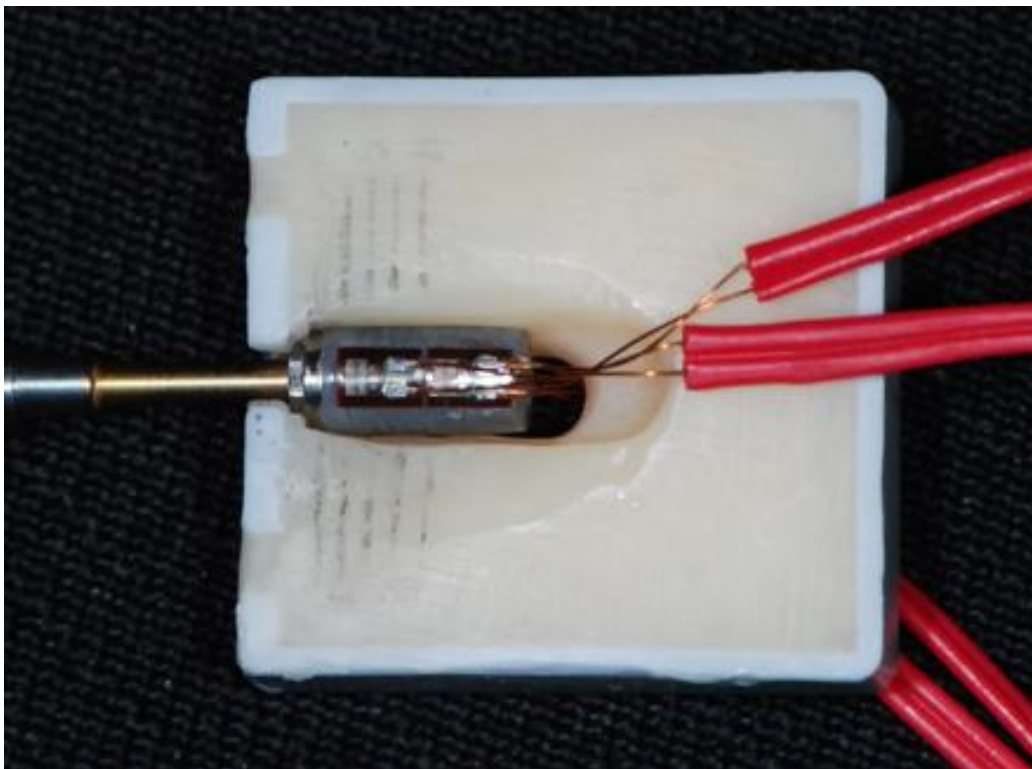


Fig. 10: Paste the strain gauge on the scaled table.

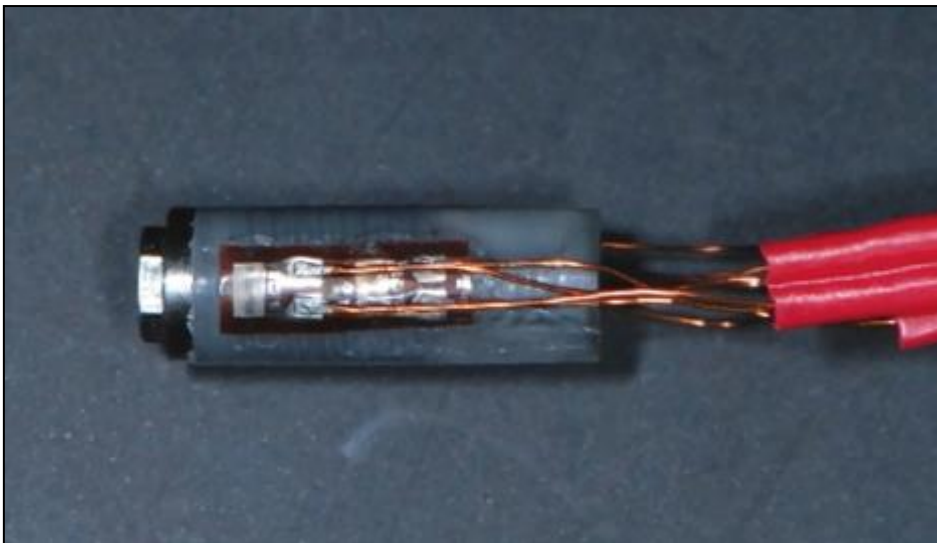
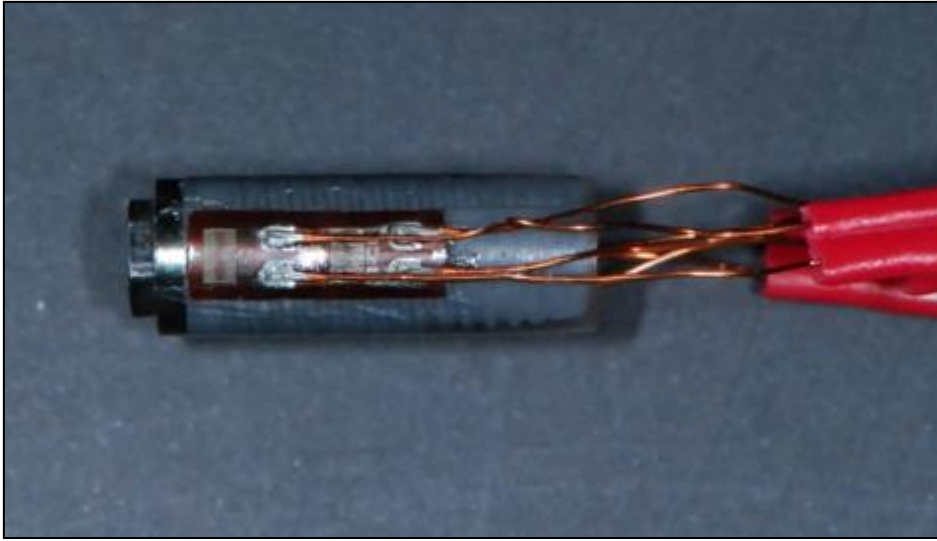


Fig. 11: Brånemark implant with strain gauges pasted.

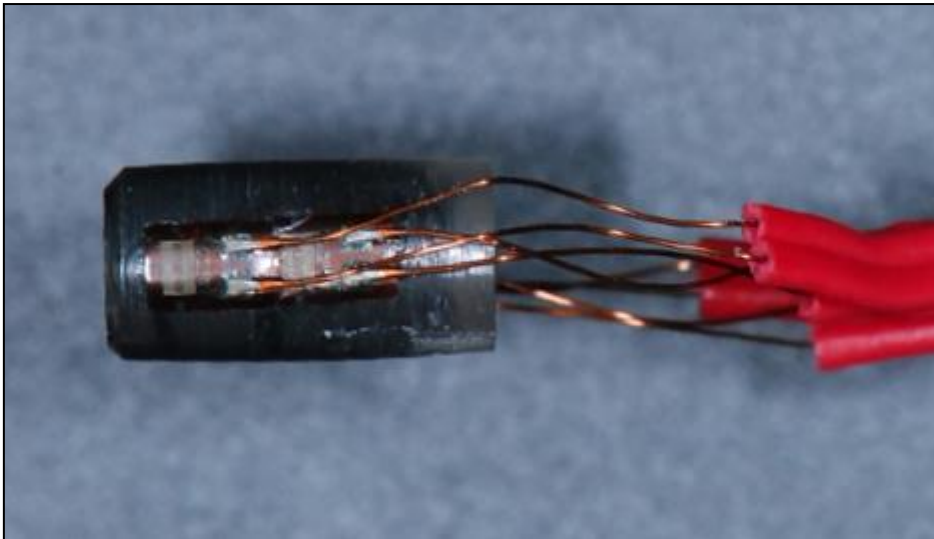
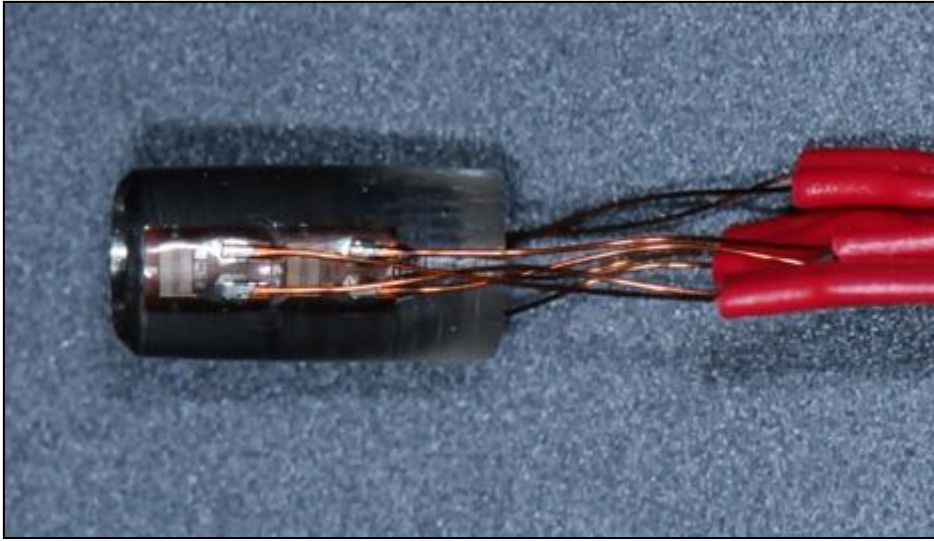


Fig.12: Astra Tech implant with strain gauges pasted.



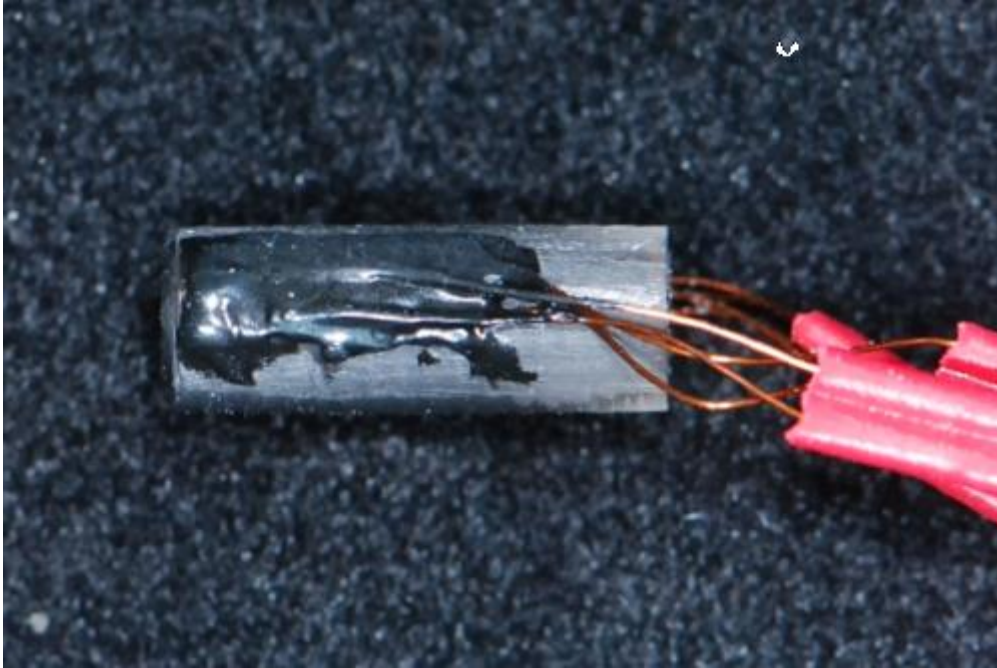


Fig. 13: The surface of the strain gauge is coated with the thermal insulation suggested by the manufacturer.



Fig. 14: 85\*20\*30 mm<sup>3</sup> rectangular block of die stone.

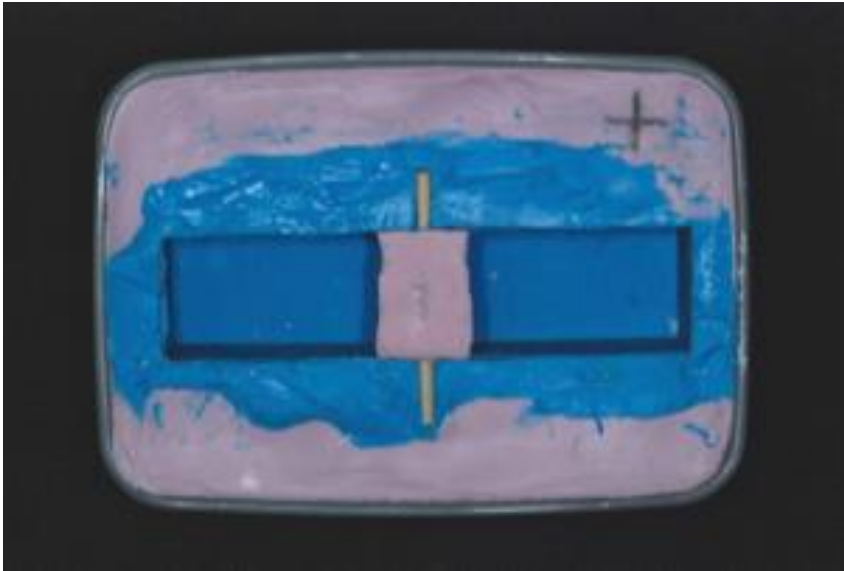


Fig. 15: The model mode made of additional silicone.

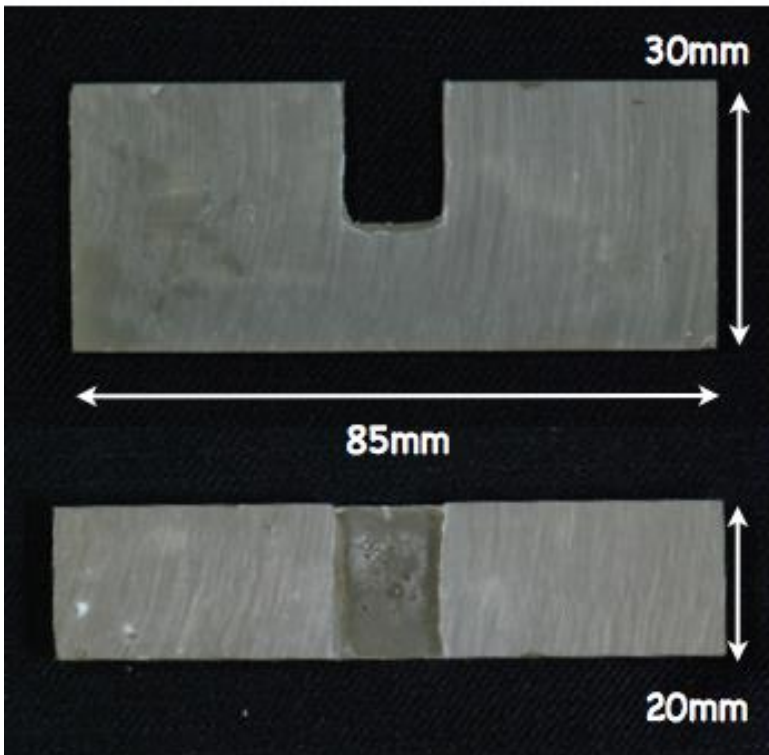


Fig. 16: The main body of PMMA resin model.

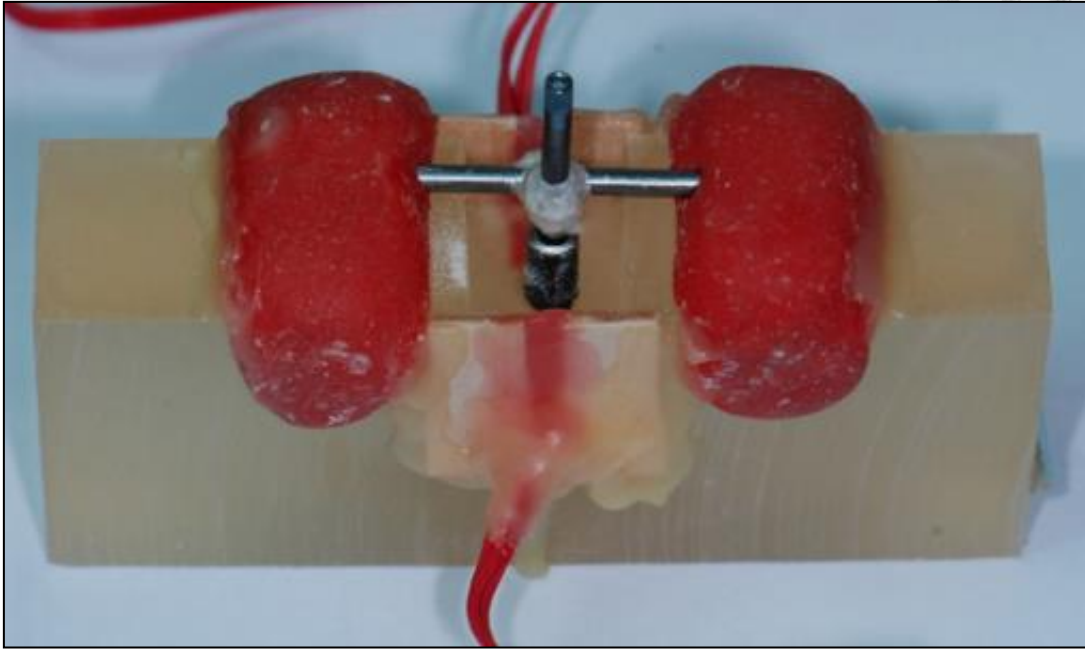


Fig. 17: The surveyed implant is connected with the prosthetic screwdriver, then fix with the metal crossbar and set them in the DuraLay stands.

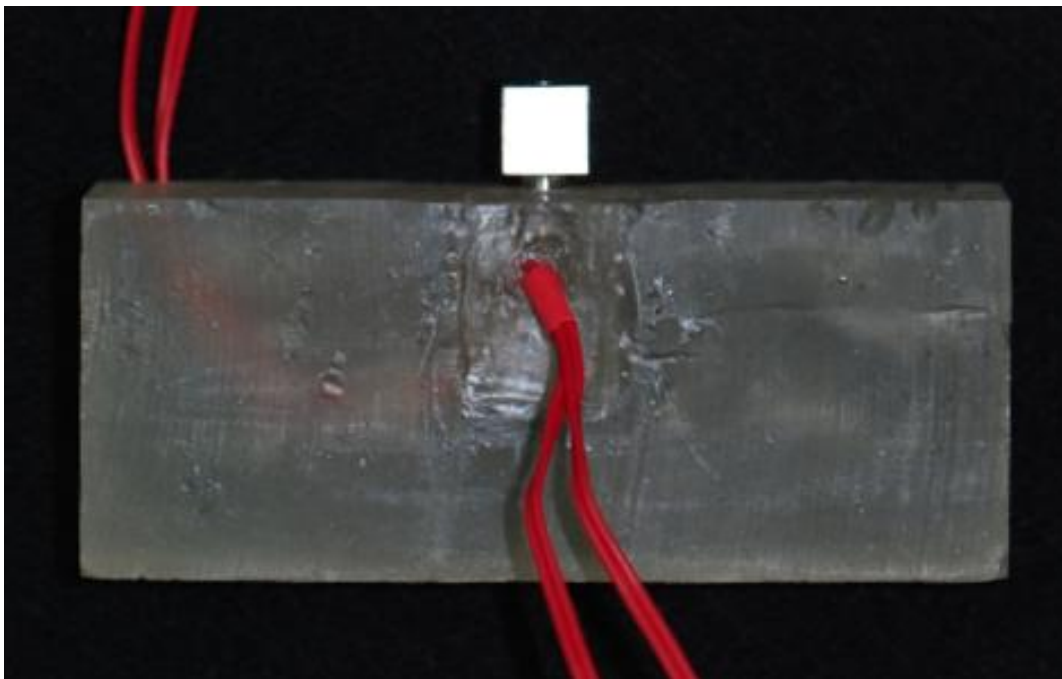


Fig. 18: The completed Brånemark model with  $8 \times 8 \times 8 \text{ mm}^3$  titanium abutment tooth.

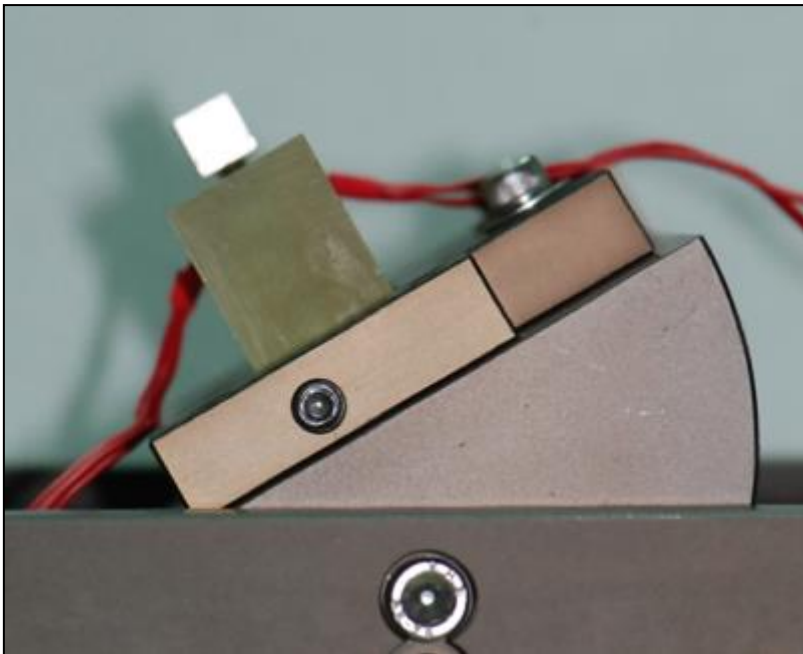


Fig. 19: Metal stage design can rotate  $360^\circ$  horizontally and  $0^\circ \pm 60^\circ$  vertically.

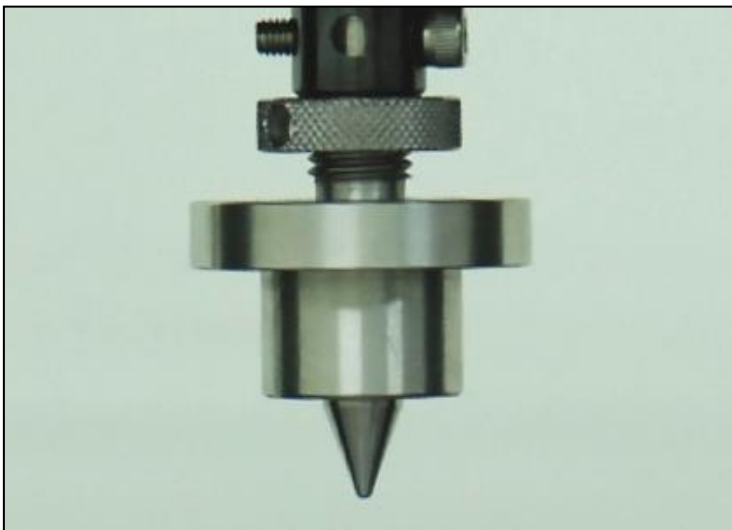


Fig. 20: Loading instrument: Instron 5566 and the loading point with a circular plane of 0.5 mm radius.

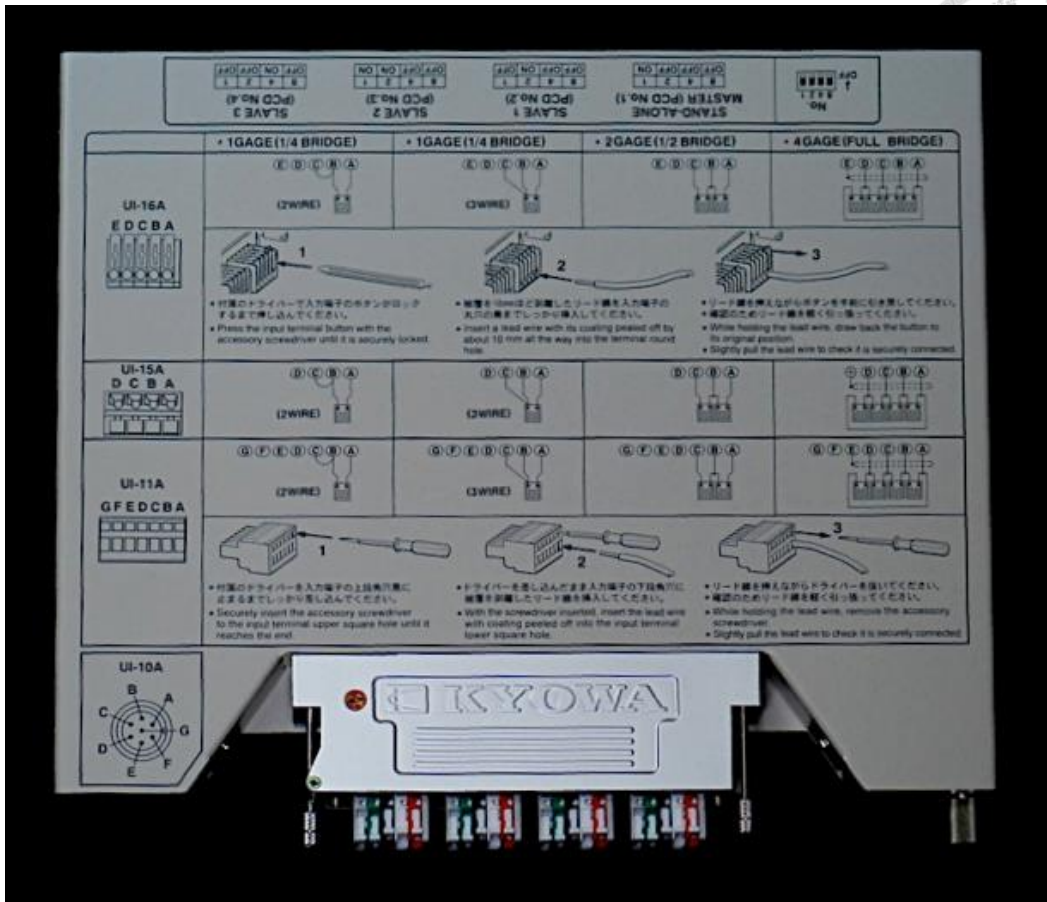


Fig. 21: Signal convertor: Kyowa PCD 300B.

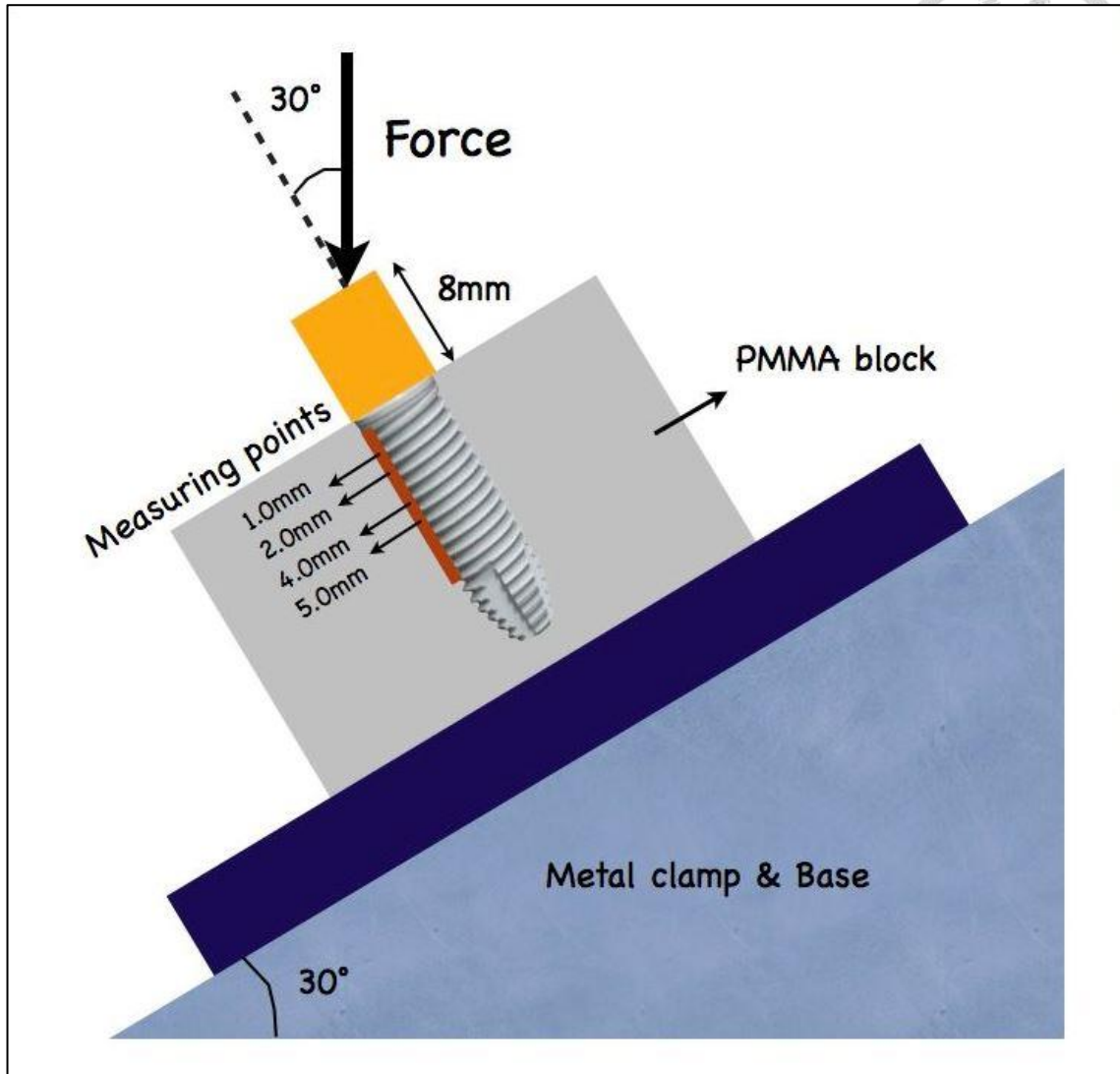
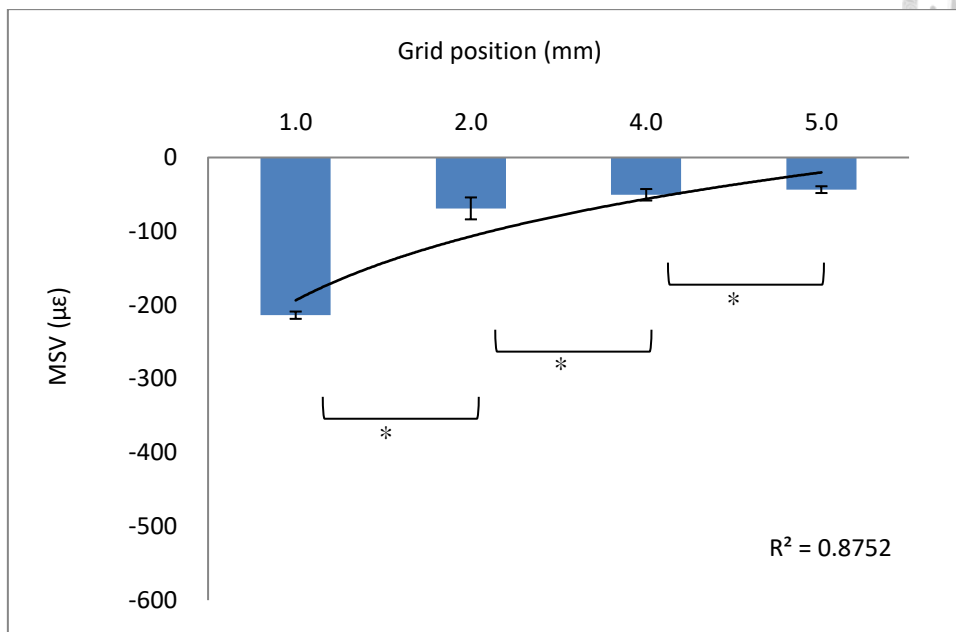


Fig. 22: The cartoon diagram of the model and force: here shows the strain gauges are under pressure during the measurement and draw all strain gauges on the same side. In fact, there are only two strain gauges at each side of the implant. The test condition as the diagram is achieved by changing the vertical angle of the metal stage.



(a)



(b)

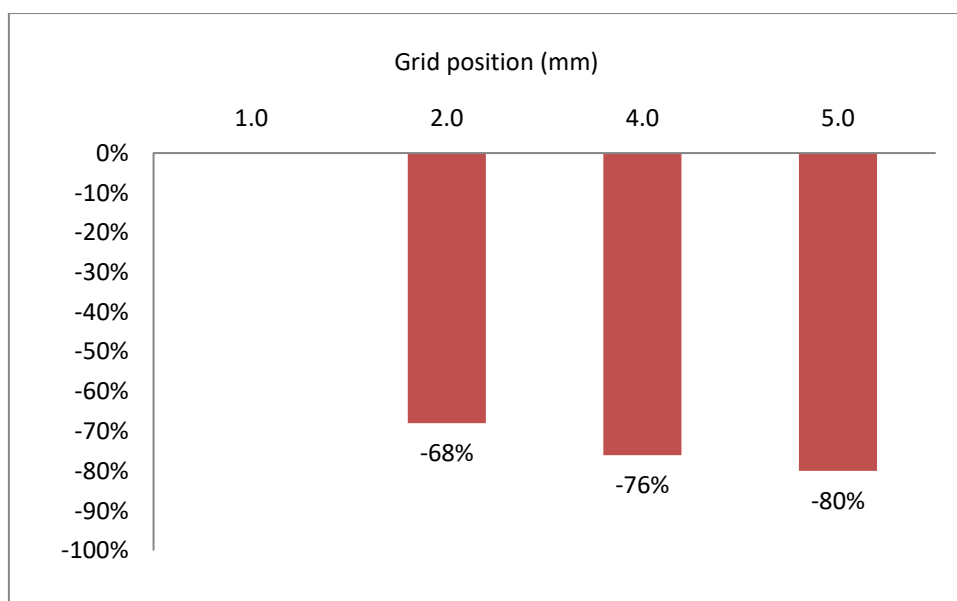
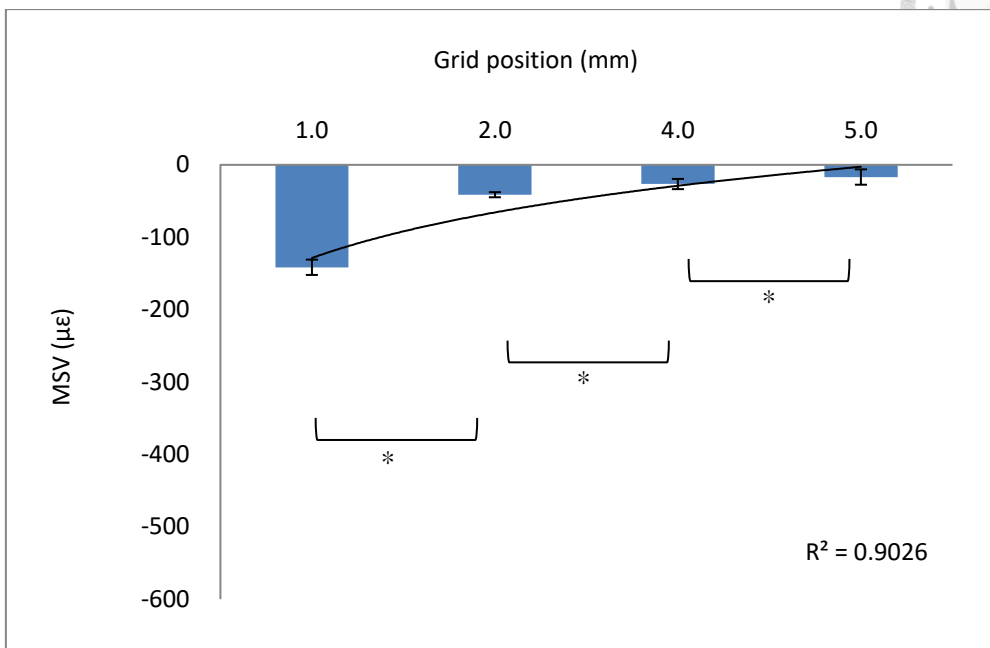


Fig. 23: 5.0\*8.5 mm Brånemark implant: (a) the MSV of micro-strain gauges at four different heights. The error bar is the positive and negative standard deviation of each group of data. The  $R^2$  of logarithmic regression line is 0.875; (b) the MSV decreasing rate of the three strain gauges below 1.0 mm. The largest value occurs at the 2.0 mm.





(a)



(b)

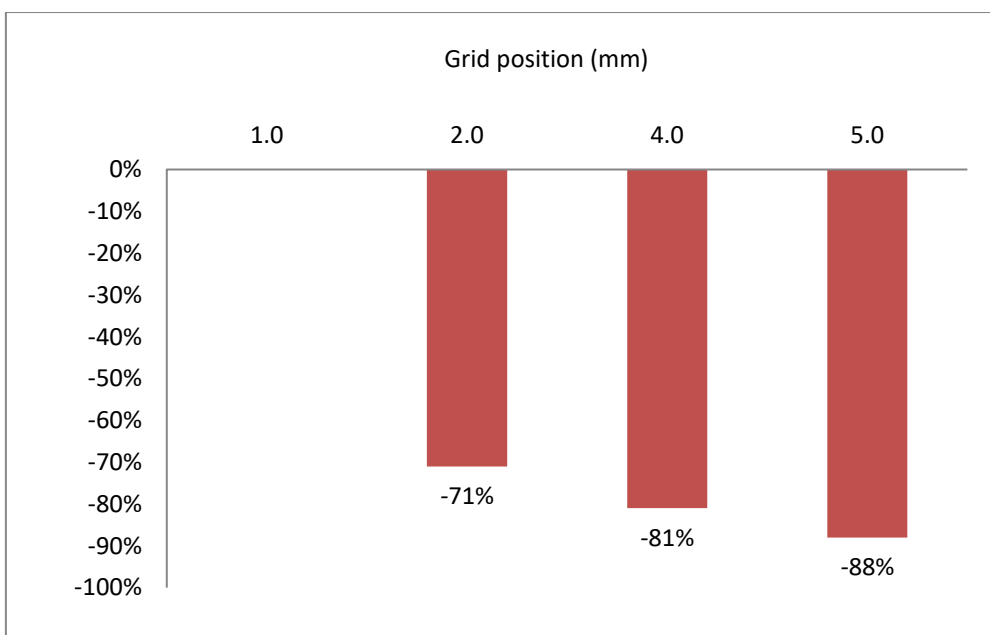
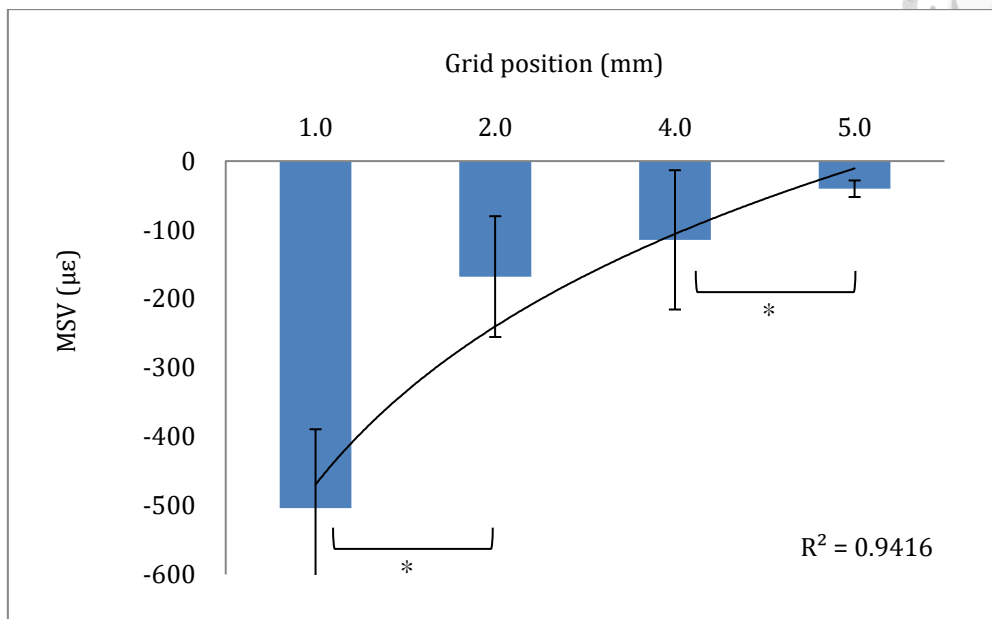


Fig. 24: 5.0\*10.0 mm Brånemark implant: (a) the MSV of micro-strain gauges at four different heights. The error bar is the positive and negative standard deviation of each group of data. The  $R^2$  of logarithmic regression line is 0.902; (b) the MSV decreasing rate of the three strain gauges below 1.0 mm. The largest value occurs at the 2.0 mm.



(a)



(b)

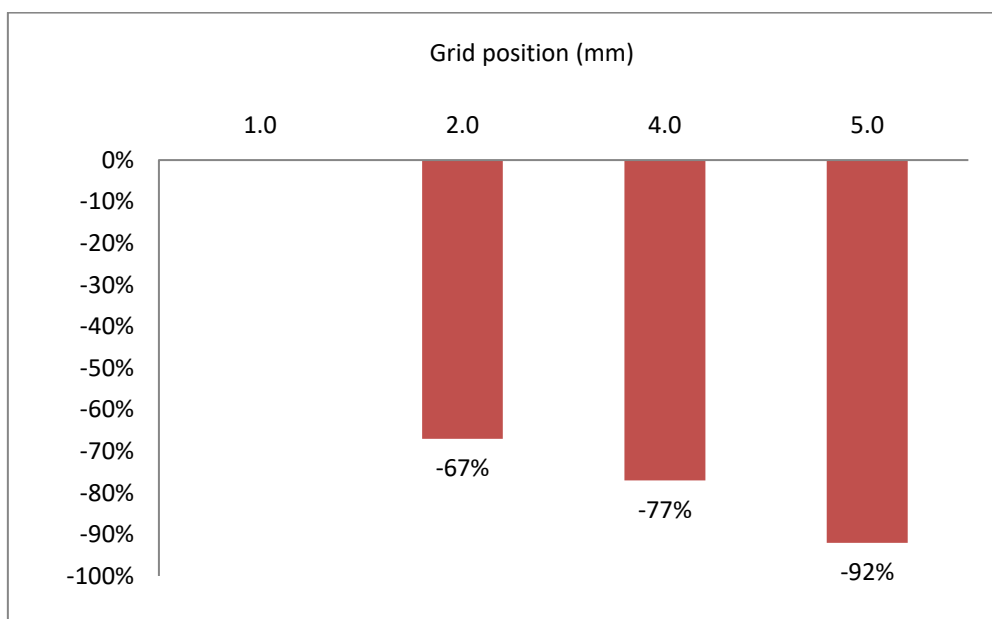
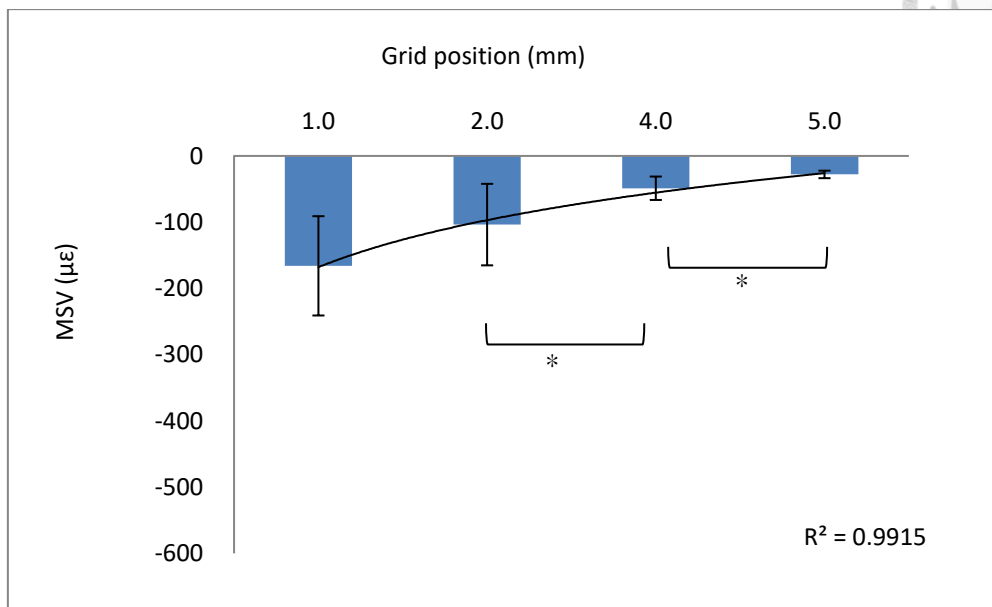


Fig. 25: 3.75\*8.5 mm Brånemark implant: (a) the MSV of micro-strain gauges at four different heights. The error bar is the positive and negative standard deviation of each group of data. The  $R^2$  of logarithmic regression line is 0.941; (b) the MSV decreasing rate of the three strain gauges below 1.0 mm. The largest value occurs at the 2.0 mm.



(a)



(b)

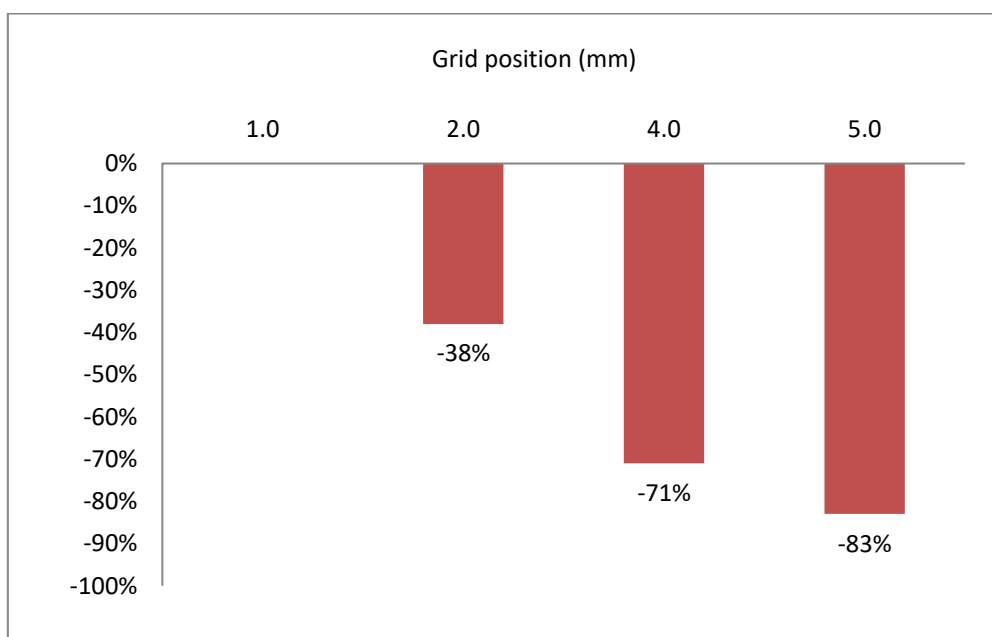
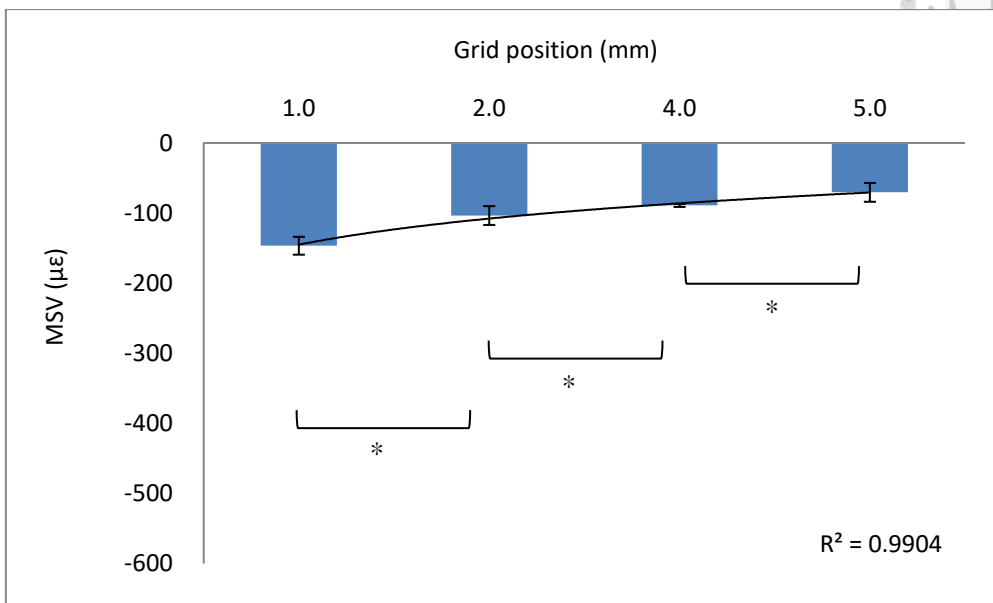


Fig. 26: 3.75\*10.0 mm Brånemark implant: (a) the MSV of micro-strain gauges at four different heights. The error bar is the positive and negative standard deviation of each group of data. The  $R^2$  of logarithmic regression line is 0.991; (b) the MSV decreasing rate of the three strain gauges below 1.0 mm. The largest value occurs at the 2.0 mm.



(a)



(b)

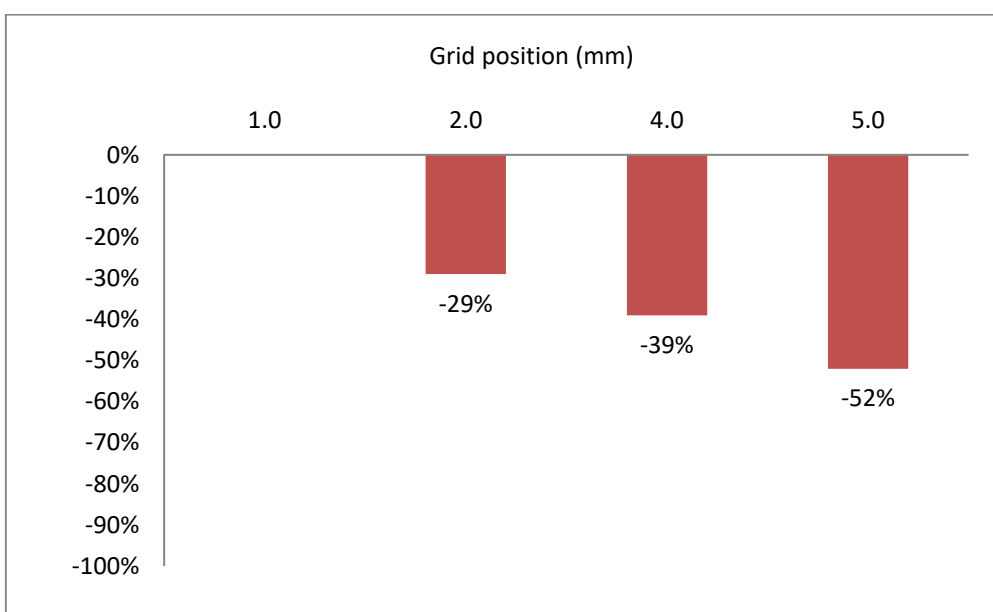
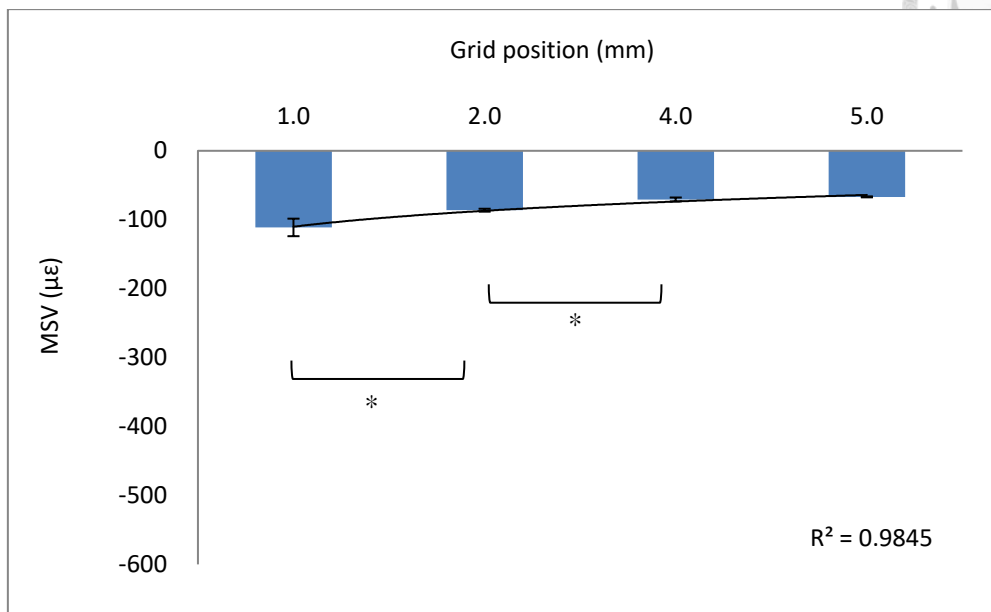


Fig. 27: 5.0\*9.0 mm Astra Tech implant: (a) the MSV of micro-strain gauges at four different heights. The error bar is the positive and negative standard deviation of each group of data. The  $R^2$  of logarithmic regression line is 0.990; (b) the MSV decreasing rate of the three strain gauges below 1.0 mm. The largest value occurs at the 2.0 mm.



(a)



(b)

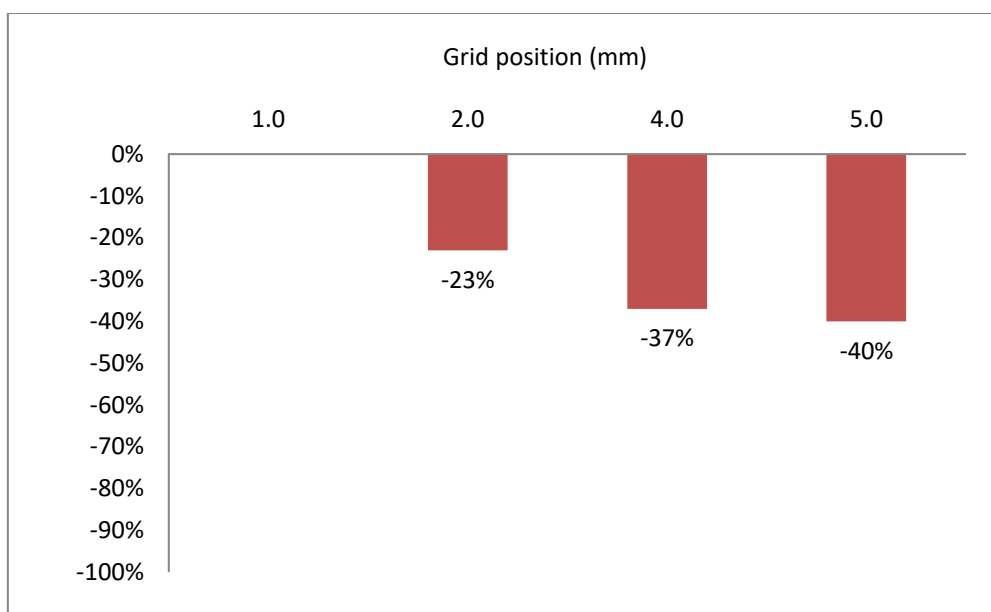
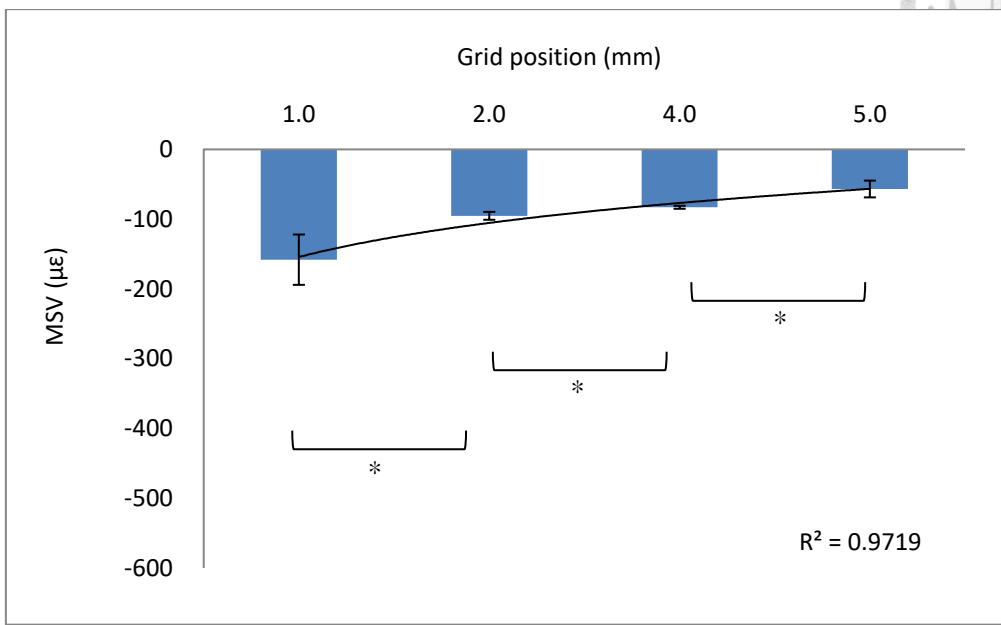


Fig. 28: 5.0\*11.0 mm Astra Tech implant: (a) the MSV of micro-strain gauges at four different heights. The error bar is the positive and negative standard deviation of each group of data. The  $R^2$  of logarithmic regression line is 0.984; (b) the MSV decreasing rate of the three strain gauges below 1.0 mm. The largest value occurs at the 2.0 mm.



(a)



(b)

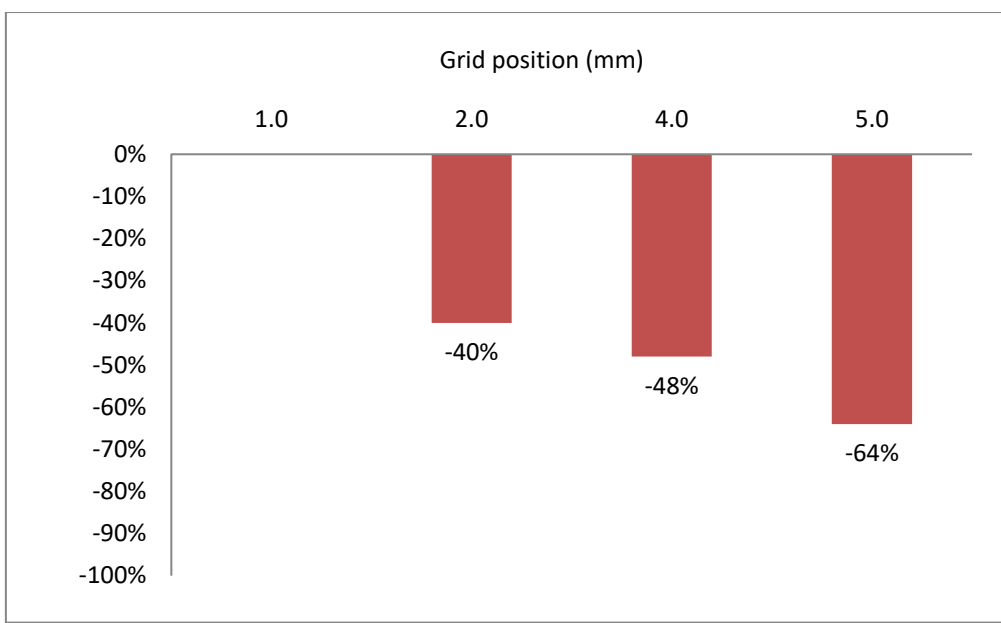
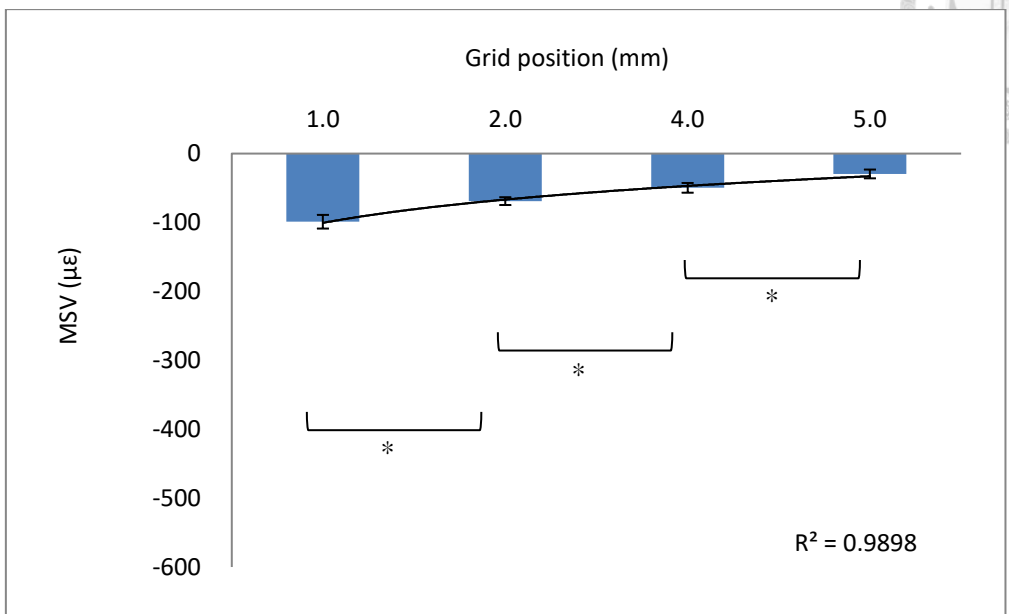


Fig. 29: 5.0S\*9.0 mm Astra Tech implant: (a) the MSV of micro-strain gauges at four different heights. The error bar is the positive and negative standard deviation of each group of data. The  $R^2$  of logarithmic regression line is 0.971; (b) the MSV decreasing rate of the three strain gauges below 1.0 mm. The largest value occurs at the 2.0 mm.



(a)



(b)

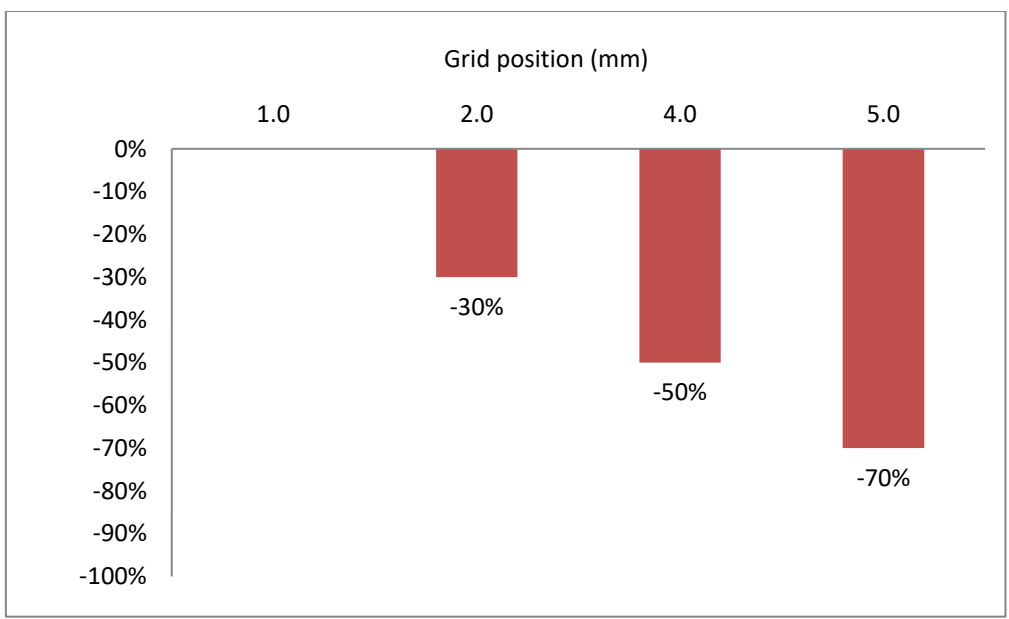
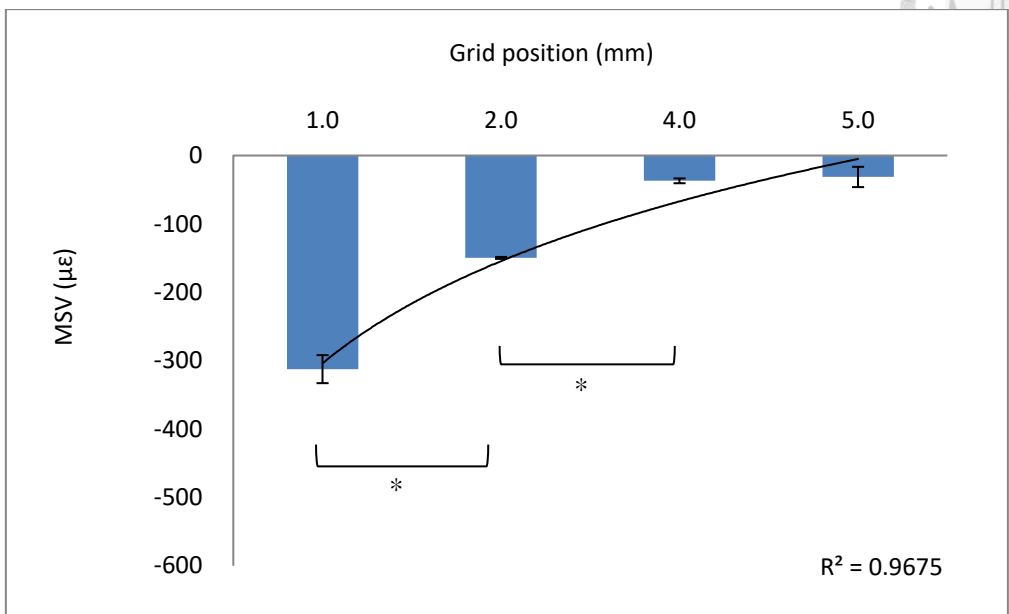


Fig. 30: 5.0S\*11.0 mm Astra Tech implant: (a) the MSV of micro-strain gauges at four different heights. The error bar is the positive and negative standard deviation of each group of data. The  $R^2$  of logarithmic regression line is 0.989; (b) the MSV decreasing rate of the three strain gauges below 1.0 mm. The largest value occurs at the 2.0 mm.



(a)



(b)

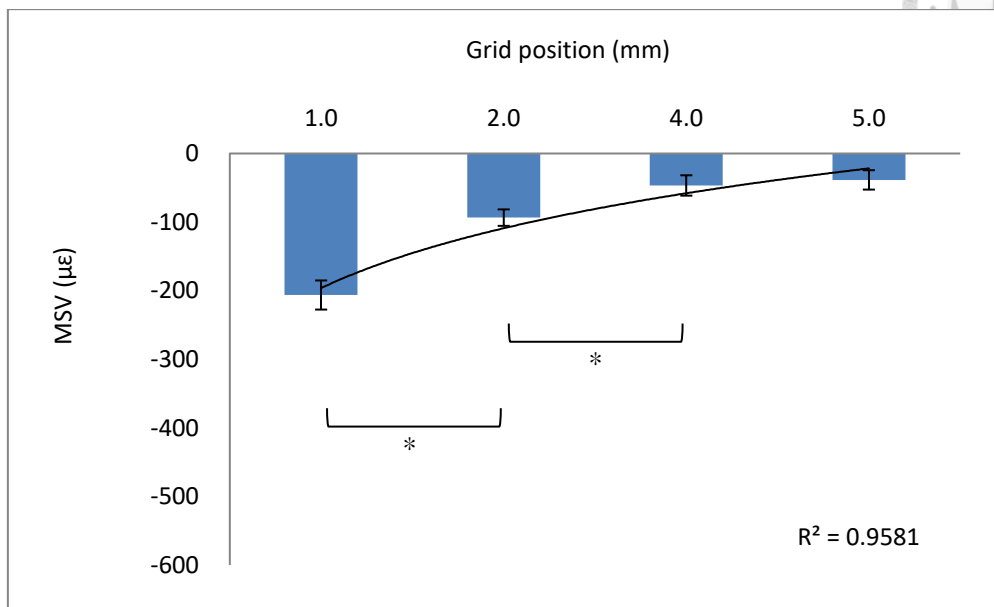


Fig. 31: 4.0S\*9.0 mm Astra Tech implant: (a) the MSV of micro-strain gauges at four different heights. The error bar is the positive and negative standard deviation of each group of data. The  $R^2$  of logarithmic regression line is 0.967; (b) the MSV decreasing rate of the three strain gauges below 1.0 mm. The largest value occurs at the 2.0 mm.





(a)



(b)

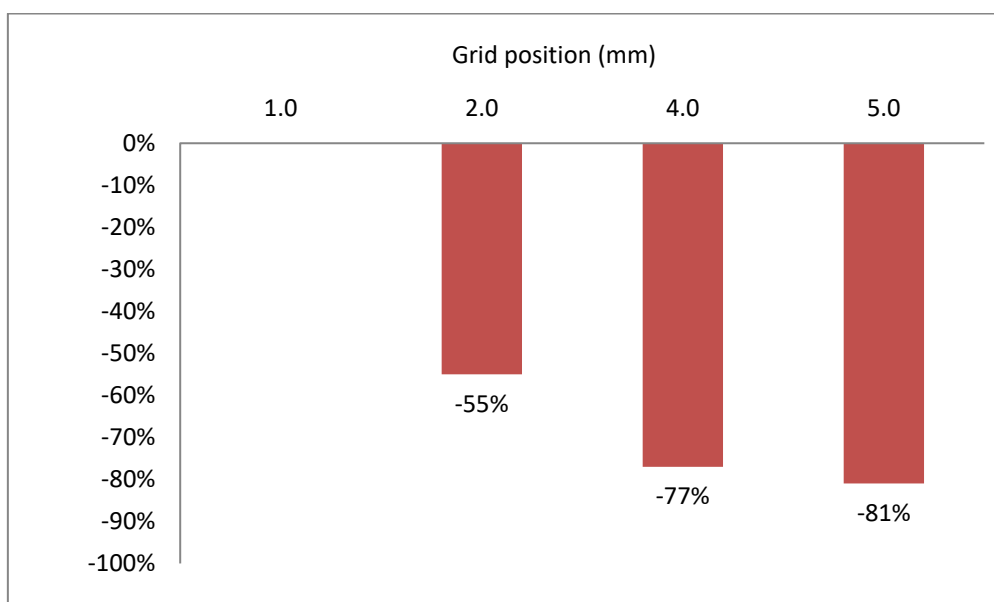


Fig. 32: 4.0S\*11.0 mm Astra Tech implant: (a) the MSV of micro-strain gauges at four different heights. The error bar is the positive and negative standard deviation of each group of data. The  $R^2$  of logarithmic regression line is 0.958; (b) the MSV decreasing rate of the three strain gauges below 1.0 mm. The largest value occurs at the 2.0 mm.

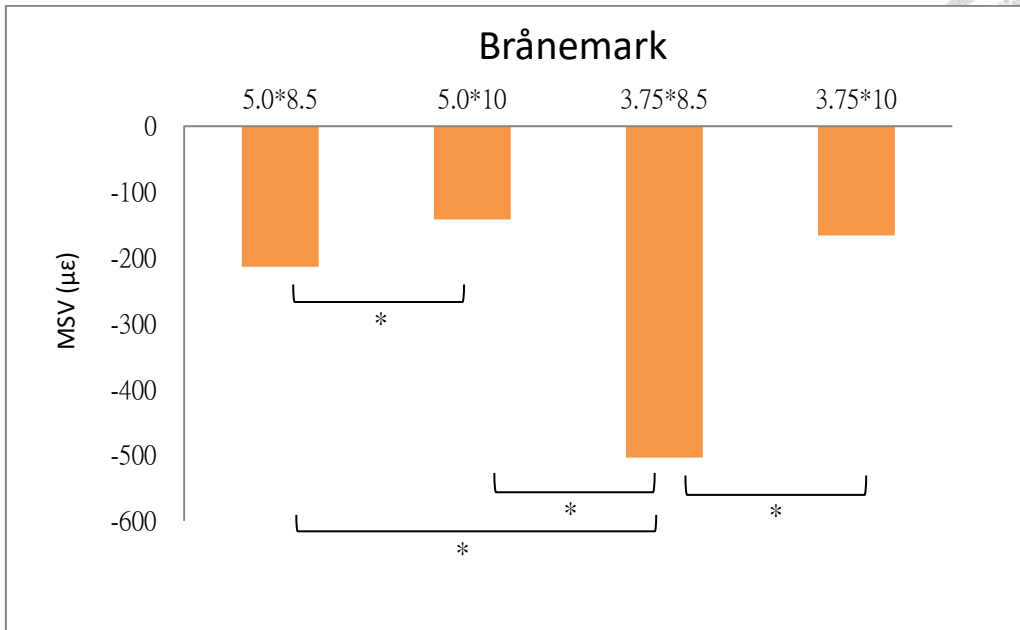


Fig. 33: The effect of the diameter and length upon stress distribution in Brånemark group at the grid position of 1.0 mm.

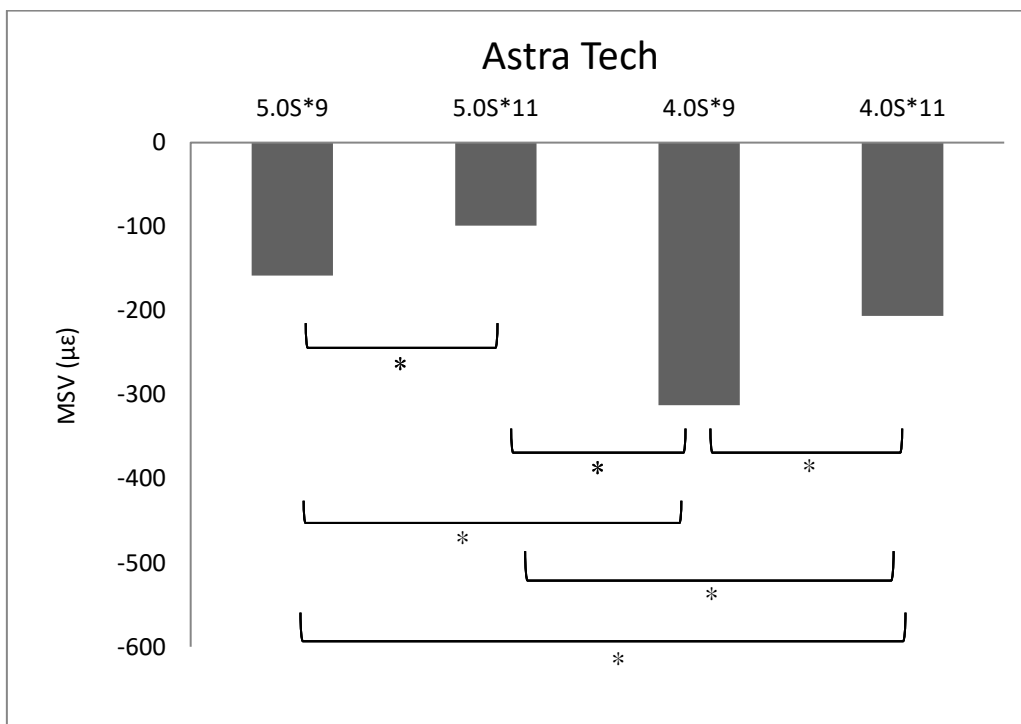


Fig. 34: The effect of the diameter and length upon stress distribution in Astra Tech group at the grid position of 1.0 mm.

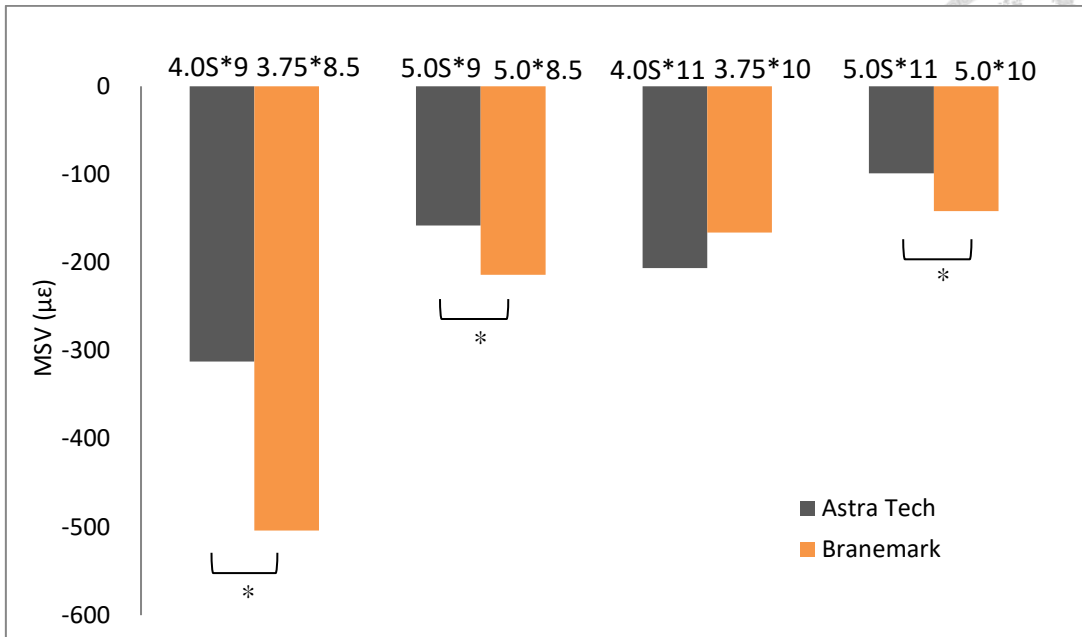


Fig. 35: The comparison of stress distribution among implants with similar diameter and length in Brånemark and Astra Tech groups.

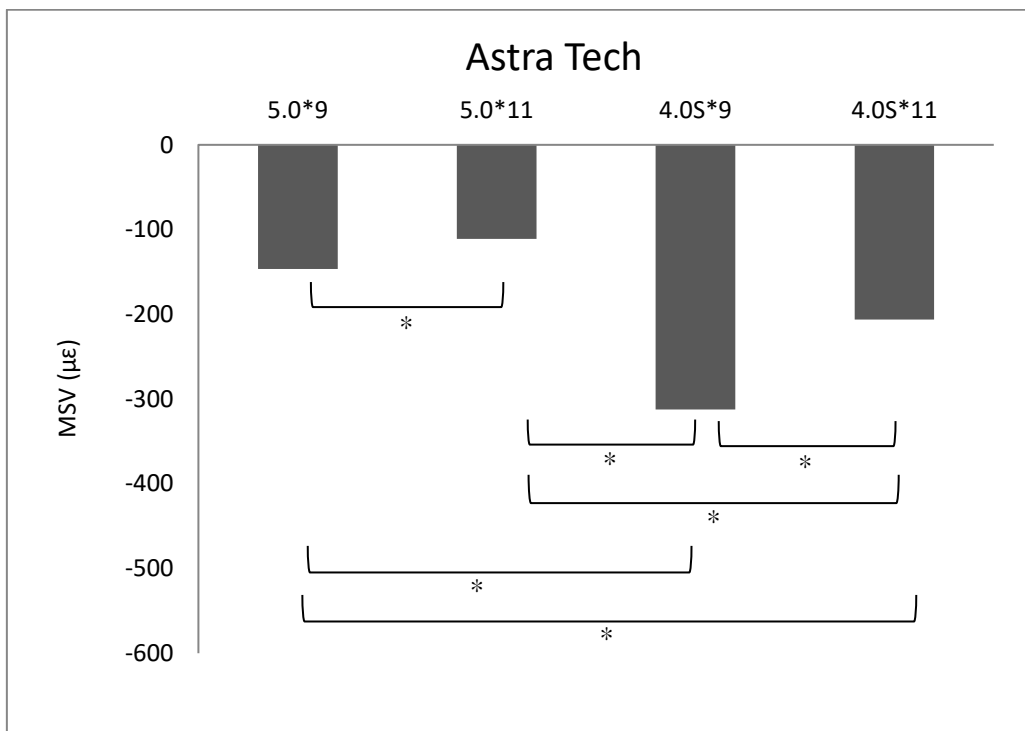


Fig. 36: The effect of the outspreaded design under the implant platform upon stress distribution in Astra Tech group.

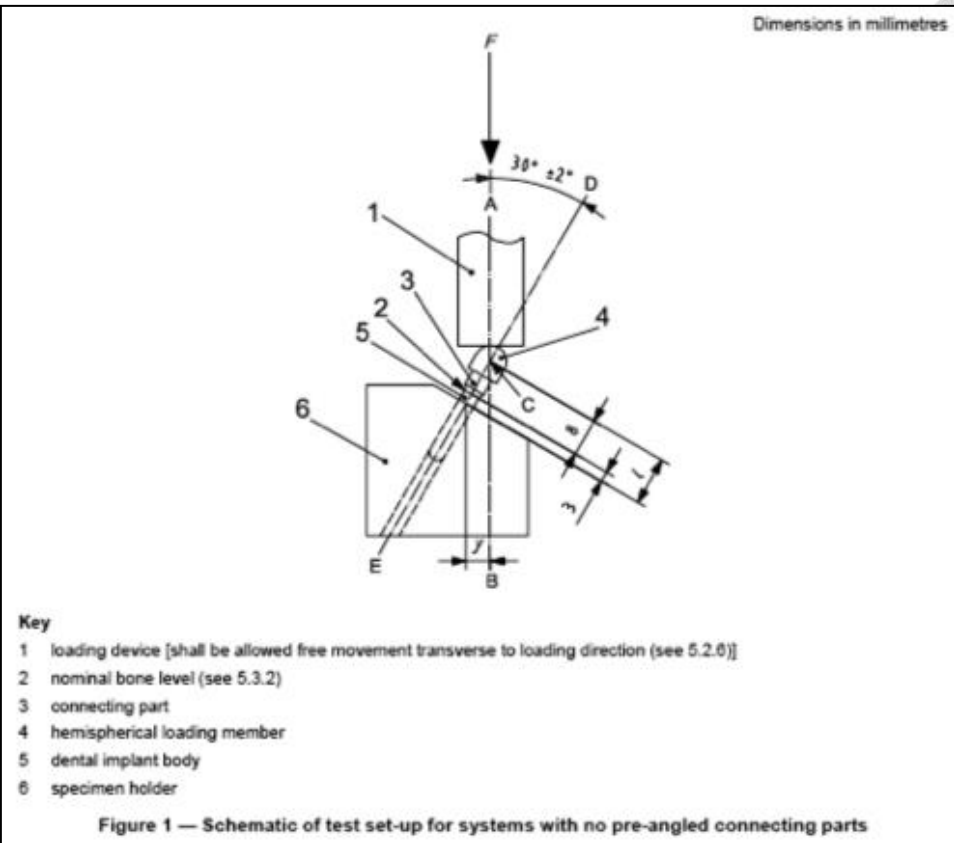


Fig. 37: The test set-up suggested by ISO for the dynamic fatigue experiment of dental implants with no pre-angled connector.

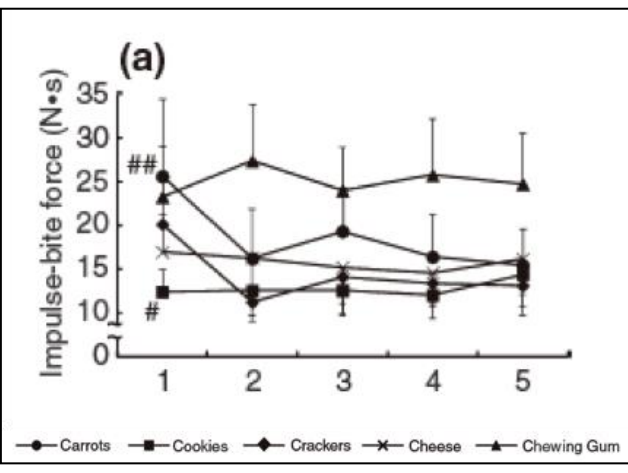


Fig. 38: The study of Shimada et al. shows the dynamic bite force of chewing 5 different kinds of food via intraoral strain gauges on the first molars of subjects.

## Tables



Grid position	Number of data	Mean	Standard deviation	Standard error	95% confidence interval of mean		Minimum value	Maximum value
					Lower limit	Upper limit		
1.0	12	-213.7500	13.57889	3.91989	-222.3776	-205.1224	-248.00	-199.00
2.0	12	-69.0000	11.33779	3.27294	-76.2037	-61.7963	-83.00	-54.00
4.0	12	-50.5417	2.16856	.62601	-51.9195	-49.1638	-54.00	-47.00
5.0	12	-43.5833	4.90748	1.41667	-46.7014	-40.4653	-50.00	-37.00
Sum	48	-94.2188	70.93643	10.23879	-114.8165	-73.6210	-248.00	-37.00

Unit:  $\mu\epsilon$

Table 1 : MSV and standard deviation of 4 different grid positions on Brånemark 5.0\*8.5 implant.

Grid position	Number of data	Mean	Standard deviation	Standard error	95% confidence interval of mean		Minimum value	Maximum value
					Lower limit	Upper limit		
1.0	12	-141.5000	4.88969	1.41153	-144.6068	-138.3932	-147.00	-131.00
2.0	12	-41.2500	2.26134	.65279	-42.6868	-39.8132	-45.00	-38.00
4.0	12	-26.5000	5.09010	1.46938	-29.7341	-23.2659	-36.00	-20.00
5.0	12	-16.8333	4.80215	1.38626	-19.8845	-13.7822	-26.00	-12.00
Sum	48	-56.5208	50.53543	7.29416	-71.1948	-41.8469	-147.00	-12.00

Unit:  $\mu\epsilon$

Table 2: MSV and standard deviation of 4 different grid positions on Brånemark 5.0\*10.0 implant.

Grid position	Number of data	Mean	Standard deviation	Standard error	95% confidence interval of mean		Minimum value	Maximum value
					Lower limit	Upper limit		
1.0	12	-503.8333	65.06198	18.78177	-545.1717	-462.4949	-583.00	-421.00
2.0	12	-167.6667	68.70931	19.83467	-211.3225	-124.0109	-240.00	-97.00
4.0	12	-114.3333	75.27445	21.72986	-162.1604	-66.5062	-193.00	-40.00
5.0	12	-40.0833	10.33492	2.98343	-46.6498	-33.5168	-53.00	-20.00
Sum	48	-206.4792	188.79517	27.25024	-261.2996	-151.6588	-583.00	-20.00

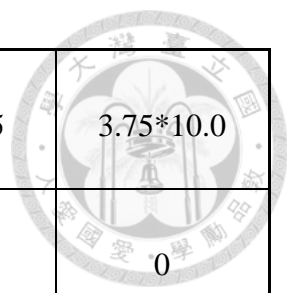
Unit:  $\mu\text{ε}$

Table 3: MSV and standard deviation of 4 different grid positions on Brånemark 3.75\*8.5 implant.

Grid position	Number of data	Mean	Standard deviation	Standard error	95% confidence interval of mean		Minimum value	Maximum value
					Lower limit	Upper limit		
1.0	12	-165.9167	60.13841	17.36046	-204.1268	-127.7065	-231.00	-105.00
2.0	12	-103.6667	48.93657	14.12677	-134.7595	-72.5739	-162.00	-53.00
4.0	12	-48.7917	11.49201	3.31746	-56.0933	-41.4900	-64.00	-37.00
5.0	12	-27.9167	4.12219	1.18997	-30.5358	-25.2976	-32.00	-21.00
Sum	48	-86.5729	66.08062	9.53792	-105.7607	-67.3851	-231.00	-21.00

Unit:  $\mu\text{ε}$

Table 4: MSV and standard deviation of 4 different grid positions on Brånemark 3.75\*10.0 implant.



Grid \ Implant	Implant			
	5.0*8.5	5.0*10.0	3.75*8.5	3.75*10.0
1.0 mm	0	0	0	0
2.0 mm	-68%	-71%	-67%	-38%
4.0 mm	-76%	-81%	-77%	-71%
5.0 mm	-80%	-88%	-92%	-83%

Table 5: MSV decreasing rate in Brånemark group: taking the MSV at the grid position of 1.0 mm as the reference value, the decreasing rate of micro-strain at the rest three positions.

Grid position	Number of data	Mean	Standard deviation	Standard error	95% confidence interval of mean		Minimum value	Maximum value
					Lower limit	Upper limit		
1.0 mm	12	-146.5833	11.26909	3.25311	-153.7434	-139.4233	-175.00	-129.00
2.0 mm	12	-103.5000	9.95901	2.87492	-109.8277	-97.1723	-118.00	-83.00
4.0 mm	12	-89.0833	7.21688	2.08333	-93.6687	-84.4979	-101.00	-75.00
5.0 mm	12	-70.4167	8.10677	2.34022	-75.5675	-65.2659	-87.00	-61.00
Sum	48	-102.3958	29.76056	4.29557	-111.0374	-93.7543	-175.00	-61.00

Unit:  $\mu\epsilon$

Table 6: MSV and standard deviation of 4 different grid positions on Astra Tech 5.0\*9.0 implant.

Grid position	Number of data	Mean	Standard deviation	Standard error	95% confidence interval of mean		Minimum value	Maximum value
					Lower limit	Upper limit		
1.0 mm	12	-111.1667	7.15838	2.06645	-115.7149	-106.6184	-121.00	-100.00
2.0 mm	12	-86.1667	7.20900	2.08106	-90.7470	-81.5863	-98.00	-74.00
4.0 mm	12	-70.5833	4.99924	1.44316	-73.7597	-67.4070	-80.00	-65.00
5.0 mm	12	-66.8333	4.30292	1.24215	-69.5673	-64.0994	-74.00	-60.00
Sum	48	-83.6875	18.57607	2.68123	-89.0814	-78.2936	-121.00	-60.00

Unit:  $\mu\text{ε}$

Table 7: MSV and standard deviation of 4 different grid positions on Astra Tech 5.0\*11.0 implant.

Grid position	Number of data	Mean	Standard deviation	Standard error	95% confidence interval of mean		Minimum value	Maximum value
					Lower limit	Upper limit		
1.0 mm	12	-158.0833	21.87343	6.31432	-171.9810	-144.1856	-183.00	-130.00
2.0 mm	12	-95.2500	3.22279	.93034	-97.2977	-93.2023	-100.00	-89.00
4.0 mm	12	-83.0000	2.52262	.72822	-84.6028	-81.3972	-88.00	-79.00
5.0 mm	12	-56.7500	8.23656	2.37769	-61.9833	-51.5167	-68.00	-47.00
Sum	48	-98.2708	39.33476	5.67748	-109.6925	-86.8492	-183.00	-47.00

Unit:  $\mu\text{ε}$

Table 8: MSV and standard deviation of 4 different grid positions on Astra Tech 5.0S\*9.0 implant.



Grid position	Number of data	Mean	Standard deviation	Standard error	95% confidence interval of mean		Minimum value	Maximum value
					Lower limit	Upper limit		
1.0 mm	12	-98.9167	11.68883	3.37428	-106.3434	-91.4899	-120.00	-80.00
2.0 mm	12	-69.0000	7.05820	2.03753	-73.4846	-64.5154	-83.00	-56.00
4.0 mm	12	-49.7500	5.06548	1.46228	-52.9685	-46.5315	-60.00	-42.00
5.0 mm	12	-29.5833	9.40462	2.71488	-35.5587	-23.6079	-44.00	-19.00
Sum	48	-61.8125	27.15492	3.91947	-69.6975	-53.9275	-120.00	-19.00

Unit:  $\mu\text{ε}$

Table 9: MSV and standard deviation of 4 different grid positions on Astra Tech 5.0S\*11.0 implant.

Grid position	Number of data	Mean	Standard deviation	Standard error	95% confidence interval of mean		Minimum value	Maximum value
					Lower limit	Upper limit		
1.0 mm	12	-312.4167	19.21391	5.54658	-324.6246	-300.2087	-337.00	-270.00
2.0 mm	12	-149.7500	19.67520	5.67974	-162.2510	-137.2490	-187.00	-128.00
4.0 mm	12	-37.0000	5.11682	1.47710	-40.2511	-33.7489	-47.00	-30.00
5.0 mm	12	-31.3333	9.36467	2.70335	-37.2834	-25.3833	-45.00	-21.00
Sum	48	-132.6250	116.12917	16.76180	-166.3454	-98.9046	-337.00	-21.00

Unit:  $\mu\text{ε}$

Table 10: MSV and standard deviation of 4 different grid positions on Astra Tech 4.0S\*9.0 implant.

Grid position	Number of data	Mean	Standard deviation	Standard error	95% confidence interval of mean		Minimum value	Maximum value
					Lower limit	Upper limit		
1.0 mm	12	-206.3333	22.33356	6.44714	-220.5234	-192.1433	-248.00	-177.00
2.0 mm	12	-93.5000	14.81707	4.27732	-102.9143	-84.0857	-127.00	-79.00
4.0 mm	12	-46.6250	8.05415	2.32503	-51.7424	-41.5076	-55.00	-31.00
5.0 mm	12	-38.5000	7.63366	2.20365	-43.3502	-33.6498	-48.00	-25.00
Sum	48	-96.2396	69.08821	9.97202	-116.3007	-76.1785	-248.00	-25.00

Unit:  $\mu\epsilon$

Table 11: MSV and standard deviation of 4 different grid positions on Astra Tech 4.0S\*11.0 implant.

Grid \ Implant	5.0*8.5	5.0*10.0	3.75*8.5	3.75*10.0
1.0 mm	0	0	0	0
2.0 mm	-29%	-23%	-40%	-30%
4.0 mm	-39%	-37%	-48%	-50%
5.0 mm	-52%	-40%	-64%	-70%

Table 12: MSV decreasing rate in Astra Tech group: taking the MSV at the grid position of 1.0 mm as the reference value, the decreasing rate of micro-strain at the rest three positions.



Grid \ Implant	4.0S*9.0	4.0S*11.0
1.0 mm	0	0
2.0 mm	-52%	-55%
4.0 mm	-88%	-77%
5.0 mm	-90%	-81%

Table 12 (continued)

(a)

Model			Length	Diameter
1	Correlation	Length	1.000	.000
		Diameter	.000	1.000
	Covariance	Length	556.248	.000
		Diameter	.000	556.248

(b)

Model	Dimension	Eigenvalue	Condition Index	Variance ratio		
				(Constant)	Diameter	Length
1	1	2.865	1.000	.01	.01	.01
	2	.100	5.353	.00	.50	.50
	3	.035	9.060	.99	.49	.49

Table 13: Collinearity diagnosis of diameter and length in Brånemark group: by (a) correlation coefficient and (b) Condition Index.

(a)

Model	R	R <sup>2</sup>	Corrected R <sup>2</sup>	Estimated Standard error	Change statistics				
					R <sup>2</sup> change	F change	df1	df2	Significant F change
1	.853a	.727	.715	81.70056	.727	60.033	2	45	.000

(b)

Model		Unstandardized coefficient		Standardized coefficient	t	Significance	95% confidence interval of B		Correlation			Collinearity statistics	
		Estimated B	Standard error	Beta distribution			Lower limit	Upper limit	Zero order	Partial	Part	Tolerance	VIF
1	Constant	-328.000	51.402		-6.381	.000	-431.529	-224.471					
	Diameter	-157.250	23.585	-.519	-6.667	.000	-204.752	-109.748	-.519	-.705	-.519	1.000	1.000
	Length	205.083	23.585	.677	8.696	.000	157.581	252.586	.677	.792	.677	1.000	1.000

Table 14: (a) coefficient of determination R<sup>2</sup> and (b) variable influence  $\beta$  of factors diameter and length in Brånemark group.



(a)

Model			Length	Diameter
1	Correlation	Length	1.000	.000
		Diameter	.000	1.000
	Covariance	Length	82.688	.000
		Diameter	.000	31.008

(b)

Model	Dimension	Eigenvalue	Condition Index	Variance ratio		
				(Constant)	Diameter	Length
1	1	2.836	1.000	.01	.02	.01
	2	.124	4.786	.01	.68	.32
	3	.041	8.347	.98	.31	.67

Table 15: Collinearity diagnosis of diameter and length in Astra Tech group: by (a) correlation coefficient and (b) Condition Index.



(a)

Model	R	R <sup>2</sup>	Corrected R <sup>2</sup>	Estimated Standard error	Change statistics				
					R <sup>2</sup> change	F change	df1	df2	Significant F change
1	.857 <sup>a</sup>	.735	.727	38.57954	.735	95.707	2	69	.000

(b)

Model	Unstandardized coefficient		Standardized coefficient	t	Significance	95% confidence interval of B		Correlation			Collinearity statistics		
	Estimated B	Standard error	Beta distribution			Lower limit	Upper limit	Zero order	Partial	Part	Tolerance	VIF	
1 Constant	-142.083	18.187		-7.813	.000	-178.365	105.802						
Diameter	-65.250	5.568	-7.26	-11.718	.000	-76.359	-54.141	-.726	-.816	-.726	1.000	1.000	
Length	66.889	9.093	.456	7.356	.000	48.748	85.029	.456	.663	.456	1.000	1.000	

Table 16: (a) coefficient of determination R<sup>2</sup> and (b) variable influence β of factors diameter and length in Astra Tech group.